SECURITY CLASSIFICATION OF THI

AD-A216 767

REPORT DOCUMENTATION PAGE

Form Approved
OMB No. 0704-0188

DTIC ELECTE JAN 12 1990 S D

a. REPORT SECURITY CLASSIFICATION: Unclassified	1b. RESTRICTIVE MARKINGS: N.A.
a. SECURITY CLASSIFICATION AUTHORITY	3. DISTRIBUTION / AVAILABILITY OF REPORT: Unlimited
2b. DECLASSIFICATION / DOWNGRADING SCHEDULE	
4. PERFORMING ORGANIZATION REPORT NUMBER(S): AFOSR-88-0339	5. MONITORING ORGANIZATION REPORT NUMBER(S): AFOSR-TR- 89-1671
6a. NAME OF PERFORMING ORGANIZATION: Johns Hopkins University; 6b. OFFICE SYMBOL (If applicable): --	7a. NAME OF MONITORING ORGANIZATION: Air Force Office of Scientific Research
6c. ADDRESS (City, State, and ZIP Code): 102 Maryland Hall, Baltimore, MD 21218	7b. ADDRESS (City, State, and ZIP Code): AFOSR, Bldg. 410-NE, Bolling AFB, DC 20332
8a. NAME OF FUNDING / SPONSORING ORGANIZATION: AFOSR; 8b. OFFICE SYMBOL (If applicable): NE	9. PROCUREMENT INSTRUMENT IDENTIFICATION NUMBER: AFOSR-88-0339
8c. ADDRESS (City, State, and ZIP Code): Bldg. 410-NE, Bolling AFB, DC 20332	10. SOURCE OF FUNDING NUMBERS: PROGRAM ELEMENT NO. 61102F; PROJECT NO. 2306; TASK NO. A1; WORK UNIT ACCESSION NO.

11. TITLE (Include Security Classification)
A Fundamental Understanding of the Effect of Alloying Elements on the Corrosion Resistance of Rapidly Solidified Mg Alloys

12. PERSONAL AUTHOR(S)
J. Kruger, G.L. Makar and K. Sieradzki

13a. TYPE OF REPORT	13b. TIME COVERED	14. DATE OF REPORT (Year, Month, Day)	15. PAGE COUNT
~~Annual~~ Final	FROM 9/30/88 TO 10/31/89	89-11-17	

16. SUPPLEMENTARY NOTATION

17. COSATI CODES			18. SUBJECT TERMS (Continue on reverse if necessary and identify by block number)
FIELD	GROUP	SUB-GROUP	Mg alloys, rapidly solidified alloys, stress corrosion, repassivation, localized corrosion

19. ABSTRACT (Continue on reverse if necessary and identify by block number)

This Final Report describes the progress achieved in the past year and includes copies of two publications resulting from a previous contract F496620-86-C-0014, P00002. The report consists of the following:
SECTION I A paper entitled "Environment-Assisted Cracking of Rapidly Solidified Mg-Al Alloys" which will be published in the Proceedings of the 11th International Congress on Corrosion, Florence, Italy, 2-9 April, 1990. This work will be continued and completed by May 1990 as part of the Ph.D. dissertation of G.L. Makar.
SECTION II A paper entitled "Structure of the Passive Films on Cast and Rapidly Solidified Mg Alloys" to be published in the Proceedings of the 11th International Congress on Corrosion, Florence, Italy, 2-9 April, 1990.
SECTION III A paper entitled "The Effect of Alloying Elements on the Corrosion Resistance of Rapidly Solidified Magnesium Alloys" which appeared in Advances in Magnesium Alloys and Composites, H.G. Paris and W.H. Hunt, Editors, TMS, Warrendale, PA, 1988, pp. 105-121.
SECTION IV A paper entitled "Corrosion Studies of Rapidly Solidified Magnesium Alloys" which will appear in the Journal of the Electrochemical Society, Vol. 137, Feb. 1990.

20. DISTRIBUTION / AVAILABILITY OF ABSTRACT	21. ABSTRACT SECURITY CLASSIFICATION
☒ UNCLASSIFIED/UNLIMITED ☐ SAME AS RPT. ☐ OTIC USERS	Unclassified
22a. NAME OF RESPONSIBLE INDIVIDUAL: ~~J. Kruger~~ Rosenstein	22b. TELEPHONE (Include Area Code): 202-767-4933; 22c. OFFICE SYMBOL: NE

D Form 1473, JUN 86 — Previous editions are obsolete. — SECURITY CLASSIFICATION OF THIS PAGE

90 01 11 119

G.W.C. Whiting
School of Engineering
The Johns Hopkins University

Materials Science and Engineering

A FUNDAMENTAL UNDERSTANDING OF THE EFFECT OF ALLOYING ELEMENTS ON THE CORROSION RESISTANCE OF RAPIDLY SOLIDIFIED Mg ALLOYS

FINAL REPORT

J. Kruger, G.L. Makar and K. Sieradzki

November 17, 1989

AFOSR-88-0339
AIR FORCE OFFICE OF SCIENTIFIC RESEARCH

INTRODUCTION

This Final Report describes the progress achieved in the past year and includes copies of two publications resulting from a previous contract F496620-86-C-0014, P00002. The report consists of the following:

SECTION I A paper entitled "Environment-Assisted Cracking of Rapidly Solidified Mg-Al Alloys" which will be published in the Proceedings of the 11th International Congress on Corrosion, Florence, Italy, 2-9 April, 1990. This work will be continued and completed by May 1990 as part of the Ph.D. dissertation of G.L. Makar.

SECTION II A paper entitled "Structure of the Passive Films on Cast and Rapidly Solidified Mg Alloys" to be published in the Proceedings of the 11th International Congress on Corrosion, Florence, Italy, 2-9 April, 1990.

SECTION III A paper entitled "The Effect of Alloying Elements on the Corrosion Resistance of Rapidly Solidified Magnesium Alloys" which appeared in Advances in Magnesium Alloys and Composites, H.G. Paris and W.H. Hunt, Editors, TMS, Warrendale, PA, 1988, pp. 105-121.

SECTION IV A paper entitled "Corrosion Studies of Rapidly Solidified Magnesium Alloys" which will appear in the Journal of the Electrochemical Society, Vol. 137, Feb. 1990.

SECTION I

ENVIRONMENT-ASSISTED CRACKING OF RAPIDLY SOLIDIFIED Mg-Al ALLOYS

G.L. Makar, J. Kruger, and K. Sieradzki
Corrosion and Electrochemistry Research Laboratory
Department of Materials Science and Engineering
The Johns Hopkins University
Baltimore, Maryland, USA 21218

ABSTRACT

Environment assisted cracking (EAC) of rapidly solidified (RS) binary Mg-Al alloys (1 and 9 wt.% aluminum) in potassium chromate/sodium chloride solutions was investigated using the constant extension rate technique (CERT) on notched ribbon samples at the open-circuit potential. The alloys were studied in the as-solidified melt-spun ribbon form. Film breakdown and repassivation properties were examined using additional electrochemical techniques. Scanning electron microscopy provided morphological information about the resultant fracture surfaces. Potential-pulse measurements showed that in both the as-cast and RS conditions, increasing aluminum content from 1 to 9 wt.% improves the repassivation rate in the chromate/chloride electrolyte. Both RS alloys repassivate quickly and completely, while their cast counterparts pass considerable charge before pitting is arrested. Constant extension rate tests conducted in the chromate/chloride environment resulted in cleavage-like fracture near the notch, while fracture in air was completely ductile.

KEYWORDS: magnesium alloys, rapid solidification, microstructure, repassivation, environment-assisted cracking, constant extension rate technique

INTRODUCTION

Magnesium is the lightest metal used in structural applications, yet it sees only limited use due to inadequate mechanical properties and high reactivity. Aluminum has long been an important alloying element for magnesium because it helps to improve both strength and corrosion resistance [1]. Among magnesium alloys, however, those containing aluminum are the most susceptible to environment-assisted cracking (EAC) [1]. Rapid solidification is a method of altering the phase constituency and microstructure of a material through systematic quenching at rates of 10^5-10^7 °C/s, several orders of magnitude faster than rates for conventional processing routes. The goal of this investigation is an understanding of the effects of both aluminum content and rapid solidification processing on EAC of Mg-Al alloys.

Cracking is primarily transgranular and may occur in a variety of electrolytes. Investigations of EAC in magnesium alloys have been conducted predominantly in electrolytes containing chloride (Cl^-) and chromate (CrO_4^{2-}) ions. Chloride is the anion most commonly responsible for localized corrosion of magnesium under service conditions, and nearly all magnesium alloys receive a chromate surface treatment to inhibit corrosion. Priest examined the effects of microstructure and pH of the chloride/chromate solution on the EAC of a Mg-6.5Al-1.0Zn-0.2Mn alloy [2]. (All alloy compositions are given in weight percent.) He concluded that decreasing the grain size and suppressing secondary phase formation always resulted in transgranular cracking, while pH had no effect. These findings were corroborated by Fairman and West, who examined a similar alloy, noting also that the transgranular stress corrosion cracking (TGSCC) was discontinuous and involved a crystallographic brittle fracture step [3]. Oryall and Tromans investigated the effect of microstructure, finding that transgranular cracks in Mg-8.6Al propagated along deformation twin boundary interfaces [4].

To concentrate on the TGSCC problem, Chakrapani and Pugh conducted a series of experiments on Mg-7.5Al using tensile specimens and bend specimens, the latter having cracks initiated in and propagating through single grains [5,6,7]. Their crystallographic analysis, acoustic emission measurements, and fractography indicated discontinuous cleavage on {3$\bar{1}$40} planes. Furthermore, they concluded the cracking they observed was a form of hydrogen embrittlement (HE). Ebtehaj et al. recently described several aspects of the EAC of Mg-7Al in solutions of varying chloride/chromate ratios ($[Cl^-]/[CrO_4^{2-}]$) [8]. They reported a minimum in the TGSCC threshold stress and maximum in crack velocity at intermediate ratios, with repassivation dominating at low $[Cl^-]/[CrO_4^{2-}]$ values and crack blunting at high values. They also reported that hydrogen embrittlement is responsible for TGSCC, and noted the importance of the repassivation process for two reasons: first, hydrogen would be expected to enter the alloy at film-free locations, and second, without exception the observed cracks initiated at pits.

The internal structure of a metallic material which has been solidified rapidly from the melt may have physical properties remarkably different from those in the as-cast form. Specific microstructural modifications may include extended solid solubility, metastable phases, fine dispersions of intermetallics, and glass formation. The underlying principles of rapid solidification processing, its effects on chemistry and microstructure, and potential applications for RS materials are described thoroughly by Jones [9]. Rapid solidification may improve corrosion resistance for several reasons: it may suppress the formation of detrimental secondary phases, the resultant chemical homogeneity may minimize local-cell action, and RS substrates may form more protective and self-healing films. With respect to general corrosion resistance, Chang et al. showed that certain Mg-Al-Zn alloys, extruded from compacted RS particulate, besides possessing high strength and ductility, have excellent resistance to corrosion in 3% NaCl solution [10]. Hashimoto and co-workers investigated resistance to localized corrosion by comparing an amorphous Fe-Cr-P-C alloy with a crystalline alloy of the same composition, finding that the films which formed on the amorphous alloy were more resistant to pitting than those on the crystalline counterpart [11]. Investigations of environment assisted cracking of RS metals and alloys, most of them metallic glasses, are described in a review by Archer et al. [12]. Although not thoroughly understood, changes in cracking behavior relative to crystalline materials apparently result from both chemical and physical effects. This paper describes exploratory experiments that examine the effects of aluminum content and RS on the EAC of magnesium alloys.

EXPERIMENTAL

The cast alloys were produced at Martin Marietta Research Laroratories in Baltimore, Maryland by melting high-purity (99.99%) magnesium and aluminum chips in graphite molds under argon at 1 atmosphere. Analyses of the Mg-1Al (A1) and Mg-9Al (A9), performed at Martin Marietta using inductively coupled plasma, are presented in Table 1. Although not all samples were analyzed for copper, all those which were contained less than 5 ppm. This material was used as-cast for certain experiments, and was also used for preparing RS samples. Samples were rapidly solidified using chill-block melt spinning. A small charge (~1.5g) of the cast material was induction melted under 1 atm. argon in a tantalum tube having an argon inlet on one side, a viewing port on the top, and a 0.6 mm orifice at the exit. When the charge was melted, argon at 7 psig was introduced into the tube, ejecting the melt onto a copper wheel rotating at 2000 rpm where it subsequently solidified as ribbon. The ribbons thus produced were about 1.5 mm wide and usually 20-30 μm thick.

Microstructures were examined using optical metallography. Both cast and RS samples were mounted in a room-temperature epoxy potting compound, polished to 0.1 μm cerium oxide, and then etched in a solution of water, diethylene glycol, and nitric acid. Optical micrographs of the as-cast A1 and A9 are shown in Figs. 1 and 2, respectively. The 1% Al alloy is a single-phase material, and polarized light was required to observe the grain structure (Fig. 1.) The alloy containing 9% Al has a more complex microstructure, having a

Table 1 - Composition of the cast Mg-1Al and Mg-9Al alloys. RS alloys were produced from this material.

	Al(wt.%)	Si(ppm)	Mn(ppm)	Fe(ppm)	Cu(ppm)
Mg-1Al (A1)	1.03	< 100	40	30	----
Mg-9Al (A9)	9.42	< 100	35	30	< 5

high concentration of the β-phase $Mg_{17}Al_{12}$ (dark regions), which transforms into a lamellar type structure as Al-rich regions formed during melting undergo a eutectoid-like decomposition [13]. Note also the dendritic aluminum-rich coring which forms around the grains. The microstructures of the RS A1 and A9 could not be resolved using optical microscopy, demonstrating the refinement inherent to this processing route. Joshi and Lewis reported that similar alloys (eg. Mg-14.4Al) contained sub-micron sized grains near the chill surface, columnar grains in the center, and equiaxed grains a few μm across near the free surface [14]. They also identified precipitates of $Mg_{17}Al_{12}$ using transmission electron microscopy, and found their ability to resolve the grain structure of the ribbons decreased with increasing Al content. Thickness measurements indicate a faster cooling rate for the RS ribbons described in the present study. This would result in more refined microstructures, and may explain our inability to resolve them using optical microscopy.

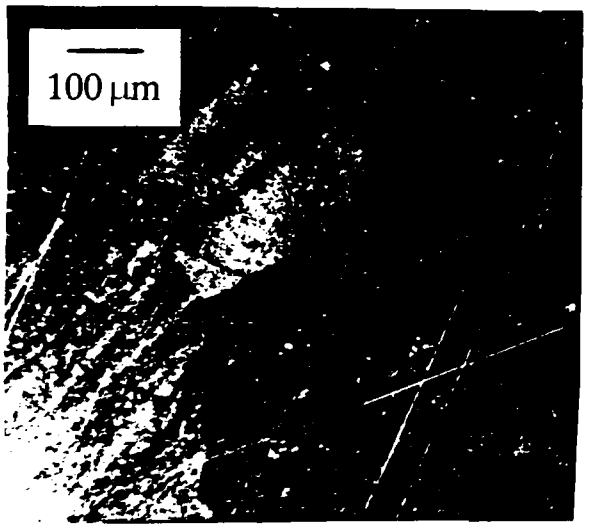

Fig.1 - Optical micrograph of cast alloy A1 (Mg-1Al), polished and etched.

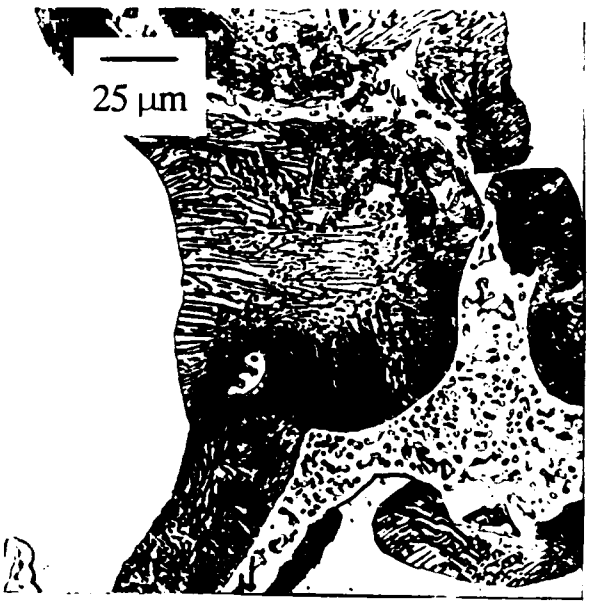

Fig.2 - Optical micrograph of cast alloy A9 (Mg-9Al), polished and etched.

Unless stated otherwise, the experiments were conducted at room temperature (24 °C)in aqueous solutions of 40 g/l potassium chromate and 35 g/l sodium chloride. The pH of this electrolyte is 9.0. Automated measurement systems were used for the electrochemical experiments. Anodic polarization scans were conducted potentiodynamically at 0.1 mV/s in a standard glass flask containing approximately 800 ml of solution. Scans were started at the open-circuit potential (E_{oc}), which was stable to within a few millivolts after about 3 hours. Repassivation was studied using a potential-pulse technique, which involved a 2-second potential of -500 mV SCE, followed by a return to the open-circuit potential and current measurements at 0.5 second intervals. A single E_{oc} value was used for each alloy

composition: -1.510 V vs. SCE for A1 and -1.475 V vs. SCE for A9. Fluctuations in E_{oc} occurred, but these were generally centered about the above values (-1.510 or -1.475 V). A platinum gauze was used as the auxillary electrode, and a saturated calomel electrode (SCE) served as the reference in all electrochemical experiments.

All samples were prepared for electrochemical tests by mounting in room-temperature epoxy with an insulated wire attached, leaving an approximately planar exposed surface of 0.3-0.6 cm^2. Ribbon samples were prepared by laying the ribbon on the partially cured epoxy, attaching the wire with silver paint after the epoxy was completely cured, then covering this contact with more epoxy. Results are reported only for the non-contact surface of the ribbons because this side possesses greater chemical homogeneity and less likelihood of contamination from the wheel. Cast samples were polished to 400-grit SiC before measuring the surface area to the nearest 0.01 cm^2. The samples were then polished to 600-grit SiC, rinsed in acetone, polished chemically in a 33% nitric acid in methanol solution, rinsed in millipore water, then dried in a stream of argon. Ribbon surfaces were prepared in the same manner, but without any physical polishing steps.

Constant extension rate tests (CERT) were conducted in the same electrolyte in a machine having a fixed base and a worm gear attached to the upper sample grip. Unless stated otherwise, an extension rate of 1.36×10^{-6} in/s was used. The samples were notched with a razor blade through about half of the ribbon width. The sample width and length of the notch were measured in an optical microscope having a calibrated eyepiece. The sample was then chemically polished, rinsed, and dried as described above before being placed in the grips. The cell was made by truncating a 500 ml laboratory wash bottle, which was then equipped with a nylon tube fitting to accomodate the rod connecting the lower grip to the base of the machine. After failure, the samples were rinsed in millipore water and acetone before being place in a dessicator. They were later placed in the SEM where the thickness was measured (needed for determining cross-sectional area) and the fracture surface examined.

RESULTS AND DISCUSSION

A previous investigation included examining the effect of aluminum content on the general corrosion resistance of binary RS Mg-Al alloys [15]. These measurements were made using a.c. impedance spectroscopy at the open-circuit potential in a sodium borate buffer solution. The corrosion rate was decreased by additions of more than 15% Al. At 45 w.% Al the corrosion rate was 75% less than that of pure Mg. Due to the desire to minimize density, this study focuses on Al contents up to 20 wt.%. The first goal of the present work was to determine what effects, if any, the Al content has on localized corrosion behavior in the chromate/chloride solutions. This was done using anodic potential scans starting at E_{oc} and proceeding at 0.1 mV/s. The solution contained 0.5 wt.% sodium chloride, a level which caused no attack at E_{oc} and a well-defined breakdown potential (E_b) when pitting began. The breakdown potential shifted -1.3V SCE for pure Mg to -0.8V for 20% aluminum, suggesting resistance to pitting improves as Al content increases. The role of aluminum in the film-formation process has not yet been investigated, but we speculate, based on the superior passivity of Al and the minimal galvanic action between Mg and Al [16], that any participation by aluminum in film formation would improve its quality. The most recently reported description of this behavior, looking specifically at the role of $Mg_{17}Al_{12}$ in the corrosion of Mg-9Al-1Zn, concluded based on Auger depth profiling that the films forming in solution on this alloy are either Mg-rich or Al-rich depending on the pH [17]. Acidic (down to pH 4) solutions favored Al-oxide while alkaline (up to pH 12) solutions favored Mg-oxide.

Acknowledging the possibility that the film-repair (repassivation) process plays an important role in EAC by minimizing the exposure of unprotected metallic surface to the electrolyte, a set of experiments was performed to examine both the effects of Al content and rapid solidification on the ability of the film which forms at E_{oc} in potassium chromate/3.5% sodium chloride to repair itself after being broken down artificially by an anodic potential pulse. After a steady state E_{oc} was established, the potential was perturbed by applying a potential about 2 V above E_{oc} (E_{pulse} = -0.5V SCE) for 2 sec. while measuring the current for 10 min. Fig. 3 shows a representative curve for each of the sample types: cast A1, cast A9, RS A1, and RS A9. There was no overlap between the data sets, and on the scale shown, duplicate tests would appear to overlay closely, except for the cast A1, for which a set of four tests covered a range of up to 500 $\mu A/cm^2$ at some times.

Focusing first on the cast alloys, Fig. 3 shows that the increase in Al content from 1% to 9% improves the repassivation behavior. The initial repassivation rate (first few seconds) is the same, but pits begin propagating again on both alloys, as indicated by the increase in current density. Pitting is then arrested by the end of the experiment in the manner described by Beck for salt-film precipitation within pits [18]. This behavior is quite different from that of the RS alloys, where the potential pulse causes a greater increase in the current density as compared to the cast alloys, but the current density then decays to a low steady state value after about 30 seconds. In fact, optical microscopy suggested some RS samples did not pit at all, but experienced rapid general dissolution during the potential pulse. Fig. 4 compares the repassivation results for RS A1 and RS A9 on a more appropriate scale. While the difference is not striking, the effect of aluminum is similar to that for the cast alloys, causing a slight improvement in the repassivation behavior. The conclusion drawn from these experiments is that increasing Al content from 1% to 9% improves the repassivation rate, particularly for the cast alloys, and rapid solidification improves the repassivation behavior for both 1 % and 9% Al. These factors are potentially, but not necessarily, important to the EAC process in Mg-Al alloys, an issue which shall be discussed in more detail later.

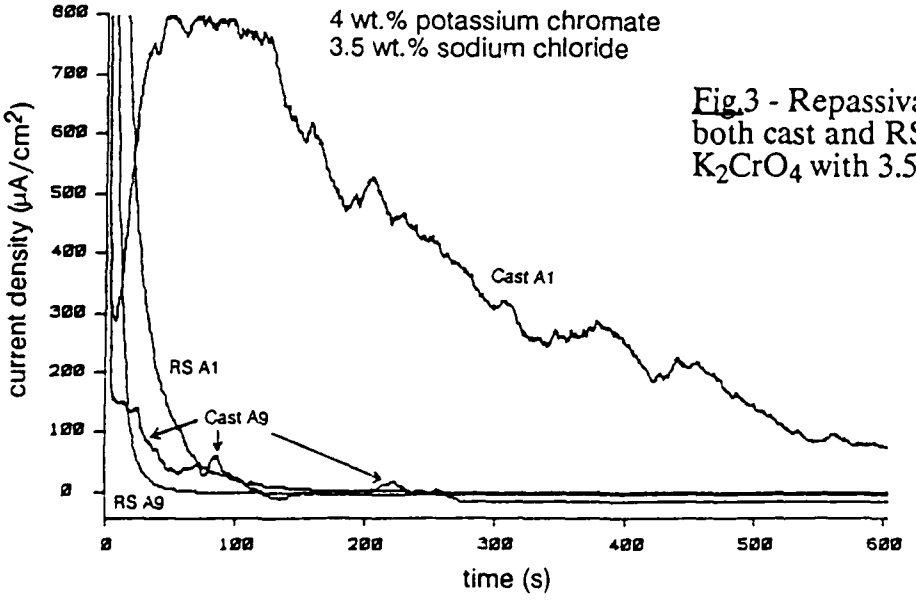

Fig.3 - Repassivation behavior for both cast and RS A1 and A9 in K_2CrO_4 with 3.5% NaCl.

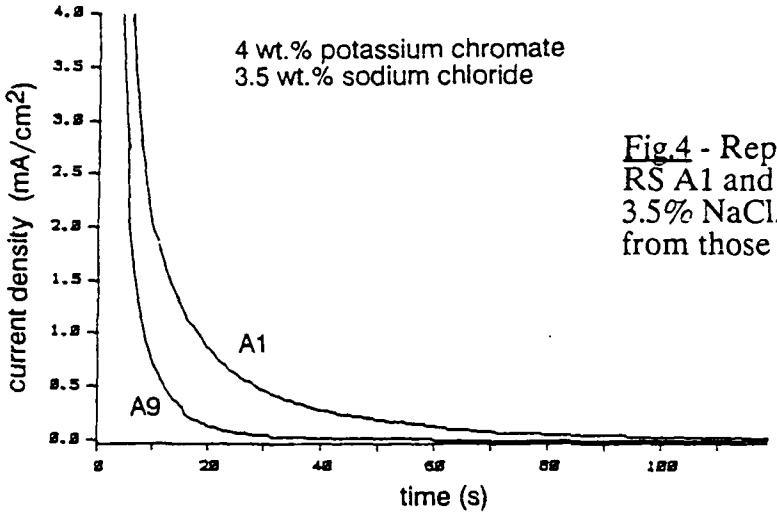

Fig.4 - Repassivation behavior for RS A1 and A9 in K_2CrO_4 with 3.5% NaCl. Both scales differ from those in Fig.6.

The CERT studies are presently in a preliminary stage, and so the results discussed here must be considered tentative. Reproducibility for the technique was examined by performing a series of four tests on alloy A1 in air at an extension rate of 10^{-5} in/s. The results were quantified using a normalized load to failure (P_f'), which includes the load to failure P_f, specimen cross-sectional area (A), and notch length (a), all of which vary from sample to sample. P_f' Was determined as follows:

$$P_f' = \frac{P_f \sqrt{a}}{A} \qquad (1)$$

The standard deviation for this series of tests was 6%, and this was considered an indication that the technique would yield results sufficiently reproducible for the measurements described here. All other tests were conducted at 1.36×10^{-6} in/s, and the results evaluated by determining P_f' and examining fracture surfaces using SEM. The chromate/chloride environment significantly lowered P_f' for both alloys, 43% for A1 and 55% for A9.

Fig. 5 shows the fracture surface of A1 in air (a) and solution (b). While significant ductility is evident in air fracture, a cleavage-type fracture is seen in the region of the notch in Fig. 5b. This cleaved region extends about 25% through the ribbon width, after which the sample fails by ductile fracture. Similar results are seen for the higher Al content alloy A9 in Fig. 6. These results show rapidly solidified A9 and A1 undergo EAC, but do not serve as a means of evaluating the effect of aluminum content. Alloy A9 is inherently stronger and less ductile than alloy A1, hence complicating the significance of load to failure. A comparison involving crack velocity may more meaningful, and subsequent experiments will compare time to failure after identifying the range of extension rates over which crack velocity is independent of stress intensity. The role of rapid solidification is being investigated with constant extension rate experiments in the same apparatus using melt-spun ribbons heat-treated to produce conventional microstructures. Fig. 7 shows the fracture surface of an A9 sample tested in solution. Prior to the experiment it was heated in an evacuated pyrex tube for 10 hours at 400 °C, and then quenched at ambient temperature. This caused significant grain growth and coarsening of β-phase particles, but did not produce the type of microstructure seen in Fig. 2. The fracture surface is considerably different than that seen for the RS A9 (Fig. 6). The cleaved surfaces, steps, and striations are characteristic of EAC fracture surfaces reported for similar cast alloys in the literature [eg. 7,19,20]. Effects of various heat treatments on the microstructure of the melt-spun ribbon

are currently being investigated. The microstructure seen in Fig. 2 has recently been produced in the melt-spun A9, but it has not yet been examined in constant extension rate tests.

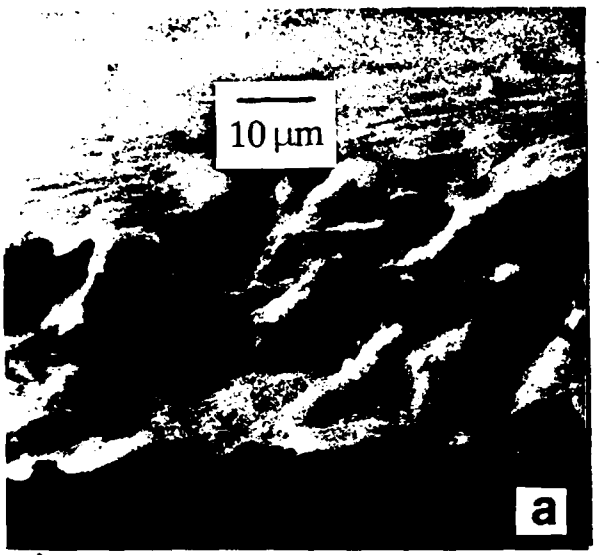

Fig.5 - SEM photomicrographs showing RS A1 fractured in air (a) and chromate/chloride solution (b).

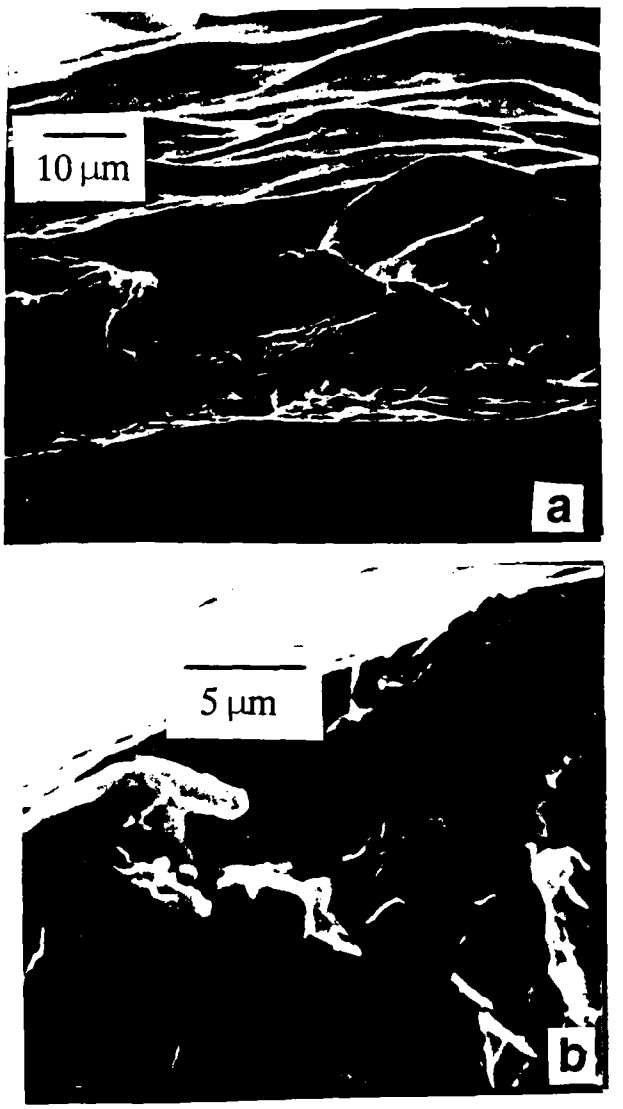

Fig.6 - SEM photomicrographs showing RS A9 fractured in air (a) and chromate/chloride solution (b).

Based on thermodynamic calculations for magnesium hydride formation [21] and results of previous investigations similar alloys [eg. 8,9], hydrogen embrittlement is probably the most likely mechanism acting in the EAC of the alloys being investigated in this study. It should be noted that cathodic polarization tends to suppress EAC of Mg-Al alloys, while it is evidence for some other alloys that HE is not the acting mechanism. The electrochemical behavior of magnesium, thoroughly covered in the literature [eg. 22,23,24] and discussed in relation to EAC of Mg-Al alloys by Ebtehaj et al., results in an increased hydrogen evolution rate when an anodic, rather than cathodic, potential is applied. Since the general electrochemical behavior of the Mg-Al alloys seems to change little upon RS , HE is probably still responsible for EAC in these alloys. Changes in the localized corrosion behavior described above, however, may play an important in the cracking process by

affecting the availability of unprotected alloy surface for hydrogen ingress. Subsequent constant extension rate experiments must therefore include examination of the effect of hydrogen content of the alloys.

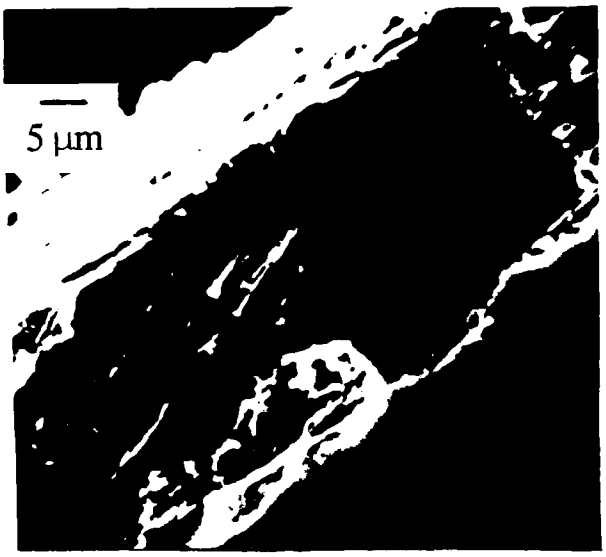

Fig.7 - SEM photomicrograph showing heat-treated RS A9 fractured in chromate/chloride solution.

CONCLUSIONS

1. For Mg-Al alloys in both the cast and RS conditions, increasing aluminum content from 1 to 9 wt.% improves the repassivation behavior in chromate/chloride solution.
2. The RS Mg-1Al and Mg-9Al alloys repassivate quickly and completely, while their cast counterparts pass a substantial amount of charge before pitting is arrested.
3. Fractography and normalized load to failure measurements show that both RS Mg-1Al and Mg-9Al undergo EAC in the chromate/chloride solution under constant extension rate conditions. The fracture surface of RS Mg-9Al differs significantly from that of a heat treated sample with a more conventional microstructure.

ACKNOWLEDGEMENTS

This work was supported by the Air Force Office of Scientific Research under contract number AFOSR-88-0339. The authors gratefully acknowledge the contributions of Dorota Artymowicz of The Johns Hopkins University, Dr. Patrick Hagans of Dow Chemical USA, Dr. Anne Joshi of the Lockheed Palo Alto Research Laboratory, Tim Langan of Martin Marietta Research Laboratories and The Johns Hopkins University, Dr. Robert Shull of the National Institute of Standards and Technology, and Walter Precht of Martin Marietta. EG&G Princeton Applied Research is a sponsor of the JHU Corrosion and Electrochemistry Research Laboratory.

REFERENCES

1. I.J. Polmear, *Light Alloys: Metallurgy of the Light Metals*, Edward Arnold Publishers Ltd., London (1981), Chapter 5.
2. D.K. Priest, in *Stress Corrosion Cracking and Embrittlement*, W.D. Robertson, ed., John Wiley, New York (1956), 81-91.
3. L. Fairman and J.M. West, *Corrosion Sci.*, 5, 711, (1965).
4. G. Oryall and D. Tromans, *Corrosion*, 29, 334, (1971).
5. D.G. Chakrapani and E.N. Pugh, *Met. Trans. A*, 6A, 1155, (1975).
6. D.G. Chakrapani and E.N. Pugh, *Corrosion*, 31, 247, (1975).
7. D.G. Chakrapani and E.N. Pugh, *Met. Trans. A*, 7A, 173, (1976).
8. K. Ebtehaj, D. Hardie, and R.N. Parkins, *Corrosion Sci.*, 28, 811, (1988).
9. H. Jones, *Materials Sci. and Engr.*, 19, 1043, (1984).
10. C.F. Chang, S.K. Das, D. Raybould, and A. Brown, *Metal Powder Rep.*, 41, 302, (1986).
11. K. Hashimoto, K. Osada, T. Masumoto, and S. Shimodaira, *Corrosion Sci.*, 16, 71, (1976).
12. M.D. Archer, C.C. Corke, and B.H. Harji, *Electrochim. Acta*, 32, 13, (1987).
13. A. Beck, *The Technology of Magnesium and its Alloys*, F.A. Hughes & Co. Ltd., London (1940), 50.
14. A. Joshi and R.E. Lewis, in *Advances in Magnesium Alloys and Composites*, H.G. Paris and W.H. Hunt, eds., TMS-AIME, Warrendale, PA, (1988), 89-103.
15. G.L. Makar, J. Kruger, and A. Joshi, in *Advances in Magnesium Alloys and Composites*, H.G. Paris and W.H. Hunt, eds., TMS-AIME, Warrendale, PA, (1988), 105-121.
16. H.H. Uhlig and R. Winston Revie, *Corrosion and Corrosion Control*, John Wiley & Sons, Inc., New York, (1985), Chapter 20.
17. O. Lunder, J.E. Lein, T.Kr. Aune, and K. Nisancioglu, *Corrosion*, 45, 741, (1989).
18. T. Beck, "Fundamental Investigation of Pitting Corrosion in Structural Metals," Report to Office of Naval Research, July 1981.
19. W.R. Wearmouth, G.P. Dean, and R.N. Parkins, *Corrosion*, 29, 251, (1973).
20. E.I. Meletis and R.F. Hochman, *Corrosion*, 40, 39, (1984).
21. G.G. Perrault, *Electroanalytical Chem. and Interfacial Electrochem.*, 51, 107, (1974).
22. P.F. King, *J. Electrochem. Soc.*, 113, 536, (1966).
23. G.A. Marsh and E. Schaschl, *J. Electrochem. Soc.*, 107, 960, (1960).
24. G.R. Hoey and M. Cohen, *J. Electrochem. Soc.*, 105, 245, (1958).

SECTION II

STRUCTURE OF THE PASSIVE FILMS ON CAST AND RAPIDLY SOLIDIFIED Mg ALLOYS

D.K. Tanaka[1] , G.G. Long[2], and J.Kruger[3]

[1]Formerly The Johns Hopkins University,
now at Instituto de Pesquisas Tecnologicas
Sao Paulo, SP, Brazil

[2]National Institute of Standards and Technology
Gaithersburg, MD 20899, USA

[3]Materials Science and Engineering, The Johns Hopkins University
Baltimore, MD 21218, USA

ABSTRACT

The structure of the passive films on cast and rapidly solidified Mg alloys was studied using the technique of EXAFS (Extended X-ray Absorption Fine Structure). A surface reflectance technique was developed (ReflEXAFS) that enabled the measurement of the thin oxide films on Mg and Mg alloys in the neighborhood of the oxygen K-edge. Surface film structures appeared to contain both MgO-like and $Mg(OH)_2$-like structure, with one or the other predominating, depending on the alloy.

KEYWORDS Mg, Mg alloys, passive films, rapidly solidified alloys, EXAFS.

INTRODUCTION

Makar and Kruger [1] recently studied the effect of alloying elements on the corrosion resistance of rapidly solidified (RS) magnesium alloys using the technique of electrochemical impedance spectroscopy to measure corrosion rate. These measurements showed that aluminum was the only element for binary alloys that caused a decrease in the corrosion rate of magnesium with increasing aluminum content. They also found when comparing cast commercial alloy AZ61 (6%Al, 1%Zn) to RS AZ61 that the RS AZ61 formed a more protective film that the cast material especially in more alkaline solutions.

About 10 years ago, Revesz and Kruger [2] suggested that a noncrystalline structure is generally more desirable for a more protective passive film than a crystalline structure. Of the many available (x-ray, neutron, and electron) scattering techniques, only x-ray absorption spectroscopy offers a direct surface-sensitive measurement of the (possibly) disordered structure of passive films on alloys. The challenge in such measurements is to study the passive film, which is often only of the order of a few nm thick, on the surface of a bulk metal or alloy containing many of the same elemental species. Two EXAFS techniques are available for surface sensitive measurements. One is partial yield electron detection, either in vacuum [3] or in the inert atmosphere of a photocathode detector [4], and the other is surface reflectance measurements [5]. The latter technique is particularly suited for measurements on ultra-thin layers of oxide on low-Z (eg. Mg) alloys because of the excellent

signal-to-noise that accompanies the surface sensitivity at moderate reflection angles. The results reported in this work were derived from surface reflectance measurements of the thin films on magnesium and magnesium alloys in the neighborhood of the oxygen K-edge.

DEVELOPMENT OF THE REFL-EXAFS TECHNIQUE

The high reflectivity of x-rays at grazing incidence to a polished surface can be described using the Fresnel equations. These equations are derived from a consideration of plane waves incident on a planar boundary. The complex dielectric permeability is given by

$$\kappa = 1 - 2\delta - 2\beta i \qquad (1)$$

The dielectric permeability determines the phase velocity of waves in the medium

$$v = \frac{c}{\sqrt{\kappa}}$$

and the complex refractive index is $n = \sqrt{\kappa}$. If both δ and β are much less than 1, then to first order

$$n = 1 - \delta - \beta i \qquad (2)$$

In this approximation, $1 - \delta$ is related to the real part of the phase velocity of the wave in the medium and β is related to the absorption that is to be measured. δ, which is called the unit decrement, is of the order of 10^{-5} - 10^{-6} for hard (~0.1 nm) x-rays, but is closer to 10^{-2} - 10^{-3} for the softer (~2.5 nm) x-rays relevant to this work. This means that second order corrections are in soft x-ray measurements. Generally, δ is always positive, so the refractive index for x-rays is less than 1. For a particular group of x-rays, the contribution to δ may be negative, as for wavelengths close to an absorption edge. Usually, however, the contributions to δ from other groups of electrons are positive so that the overall δ is still positive.

The critical angle for total reflection is defined in terms of δ as $\phi_c = \sqrt{2\delta}$. Although the reflectance is not actually equal to 1 at angles smaller than this, it can be quite high for reflectors that have negligible absorption. The behavior of the reflectance as a function of normalized glancing angle is shown for values of β/δ between zero and 1 in Fig. 1. For small values of β/δ, the value of the critical angle is defined. If the inflection point for the reflectance curve indicates the position of the critical angle, then for β/δ larger than 0.63 the reflectance curves do not show the existence of a critical angle for total reflection. The reflectance, however, is still accurately predicted by the theory.

For the present study, the values of δ and β, both of which carry EXAFS information, are calculated for magnesium oxide using equations that are valid close to the K-edge of oxygen [6,7]. Under "total" reflection conditions, there is no wave propagating into the medium. Instead, there are waves of varying amplitude (evanescent waves) present which decrease with increasing penetration. These waves enter the medium and then emerge again from the same surface. The 1/e penetration depth, d, can be calculated from the imaginary part of the reflectance.

Fig. 2 shows the penetration depth in MgO as a function of angle for a range of energies relevant to studies near the oxygen K-edge, where, for the purposes of calculation, the effects on λ are assumed to be dominated by oxygen 1s electrons. For angles less than approximately 2.3°, the penetration depth for all photon energies up to 800 eV is less than 3.0 nm. Outside the region for "total" reflection, interference can take place for a thin film on the surface of a substrate. The periodicity of the interference pattern can be used to measure the thickness of such films if they are uniform.

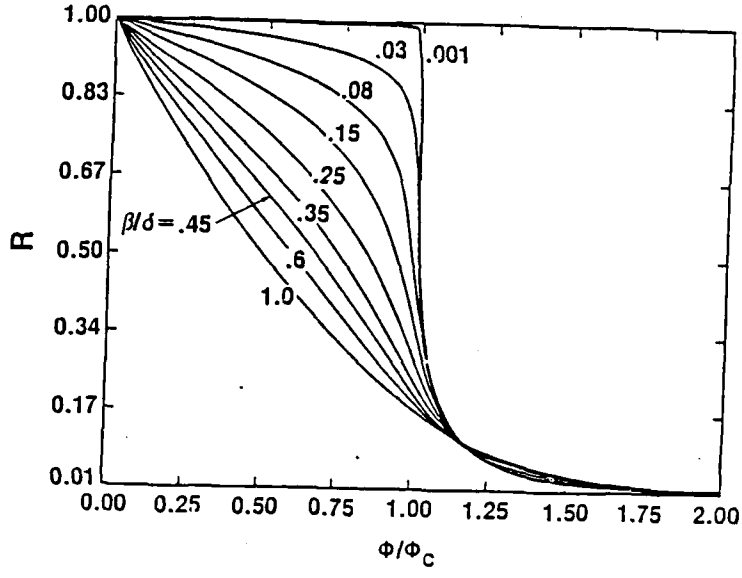

Fig. 1 - The reflectance, R, as a function of the normalized glancing angle, ϕ / ϕ_c, for different values of β / δ.

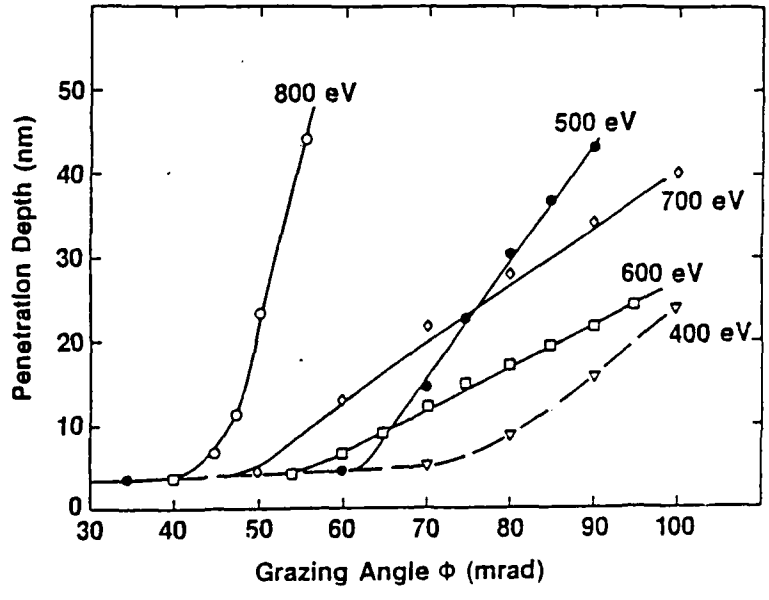

Fig. 2 - Penetration depth in MgO as a function of grazing angle, ϕ, for a range of energies.

Since the wavelengths of x-rays are about 100 times smaller than those of visible light, there is an increased concern about the smoothness of the reflecting surface. Since the glancing angle for x-rays is about 100 times smaller than for optical, the quality of the reflecting surface should be of the order of 20 times better.

EXPERIMENTAL ASPECTS

Specimens of pure Mg, AZ61 Mg alloy, Mg-15%Al, Mg-30%Al, an Mg-Al-Zn-Nd alloy from Allied Signal Corp. that was extruded from crushed rapidly solidified ribbons into bar form, and standards of single crystal MgO and $Mg(OH)_2$ were polished to a mirror-like finish. Films were formed on the Mg and Mg alloy surfaces by exposure to a humid atmosphere at 100 °C and to a borate buffer solution.

The surface reflectance measurements were performed on the U-15 beamline (SUNY/NSLS) at the National Synchrotron Light Source at Brookhaven National Laboratory. The beamline is equipped with a toroidal grating monochromator (TGM) with a 600 line/mm gold-coated grating. The TGM has a constant wavelength resolution which depends on the size of the aperture in front of the grating and on the electron beam in the storage ring.

The geometry of the refl-EXAFS experiment is shown in Fig. 3. The soft x-rays entering the sample area impinge first on a gold mesh. The remainder of the beam impinges at grazing ($0.5° < 2\phi < 3.5°$) incidence on the sample and the reflected beam is measured.

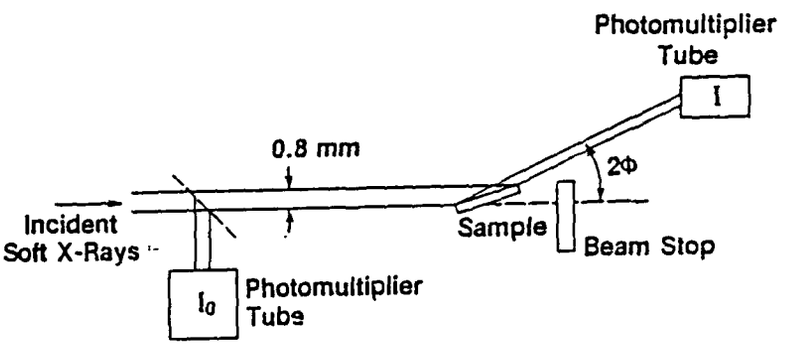

Fig. 3 - Geometry of the refl-EXAFS experiments.

A major problem in carrying out reflEXAFS measurements is the treatment of the data to remove the instrumental factors from the raw data. A considerable amount of time was spent during the past two years developing the methodology to do this. The spectral range for the measurements is from 480-1000 eV. A measure of the window transmission function over this range is provided by scans performed without the specimen in the beam. Next, corrections are made for the harmonic content in the beam intensities with and without the specimen in the beam, taking into consideration the second order reflectivity contributions. This treatment yields the EXAFS contributions that provide data on nearest neighbor distances, coordination numbers and degree of order for the Mg and O atoms in the films on the metal surface that control corrosion.

STRUCTURE OF FILMS

ReflEXAFS provides the following kinds of structural information: 1) the nearest neighbor distances (eg. for the first shell the O-Mg distance, r_1), 2) the coordination number, n_1 (for the first shell), and 3) the relative Debye-Waller factor, σ^2, a measure of the degree of structural and thermal disorder. The results obtained for pure Mg and a number of alloys and the two standards, MgO and $Mg(OH)_2$, are given in Table I. They show that there are clearly two types of surface film structures involved. The first group, represented by pure Mg and AZ61, have films whose structures and compositions are closer to MgO. AZ61, however, has a lower coordination number, suggesting greater static disorder in the film. The second group, Mg-15%Al, Mg-30%Al, and an extruded RSP alloy obtained from Allied-Signal Corp., appear to have a structure more like $Mg(OH)_2$ content in their surface films because of the larger O-Mg distances. The greatest degree of disorder was observed for the film on the RSP alloy with the Mg-15%Al alloy not far behind. This interpretation of the results is suggested by theoretical studies which tied degree of noncrystallinity to corrosion resistance[2].

TABLE I - ReflEXAFS Data

	r_1	n_1	σ^2
MgO	2.106	6.0	
$Mg(OH)_2$	2.173	3.0	
Pure Mg	2.09	2.9	0.0054
AZ61	2.09	2.3	0.0056
Mg(15%)Al	2.12	3.1	0.0134
Mg(30%)Al	2.12	2.8	0.0056
RSP Mg Alloy	2.14	1.3	0.0112

ACKNOWLEDGEMENT

We are grateful to the U.S. Air Force Office of Scientific Research for their partial support of this work under contract No.F33615-85-C-5032.

REFERENCES

1) G.L. MAKAR and J. KRUGER, J. Electrochem. Soc., 137, Feb. (1990).

2) A.G. REVESZ and J. KRUGER, Passivity of Metals, R.P. Frankenthal and J. Kruger, Eds., The Electrochemical Society, Princeton, NJ (1978) 137.

3) J. STOHR, D. DENLEY, and P. PERSETTI, Phys. Rev. B, 18 (1978) 4132.

4) G.G. LONG, J. KRUGER, D.R. BLACK, and M. KURIYAMA, J. Electroanal. Chem., 150 (1983) 603.

5) R. BARCHEWITZ, M. CREMONESE-VISICATO, and G. ONORI, J. Phys. C: Sol. St. Phys., 11 (1978) 4439.

6) A.H. COMPTON and S.K. ALLISON, X-Rays in Theory and Experiment, 2nd Ed., Van Nostrand, Princeton, NJ (1935) Chap. 4.

7) M.A. BLOKHIN, The Physics of X-Rays, 2nd Ed., State Publishing House of Technical-Theoretical Literature, Moscow (1957) Chap. 5.

SECTION III

FROM

Advances in Magnesium Alloys and Composites

Proceedings of a symposium sponsored by the International Magnesium Association and the Non-Ferrous Metals Committee, held at the Annual Meeting of the Minerals Metals and Materials Society in Phoenix, Arizona, January 26, 1988.

Edited by
Henry G. Paris
Alcoa Defense Systems, Inc.
San Diego, CA

and

W.H. Hunt
Alcoa Technical Center
Alcoa Center, PA

A Publication of
TMS
Minerals · Metals · Materials

THE EFFECT OF ALLOYING ELEMENTS ON THE CORROSION RESISTANCE OF RAPIDLY SOLIDIFIED MAGNESIUM ALLOYS

G. L. Makar and J. Kruger
Corrosion and Electrochemistry Research Laboratory
Department of Materials Science and Engineering
The Johns Hopkins University
Baltimore, Maryland 21218

A. Joshi
Lockheed Palo Alto Research Laboratory
3251 Hanover Street
Palo Alto, California 94304

Abstract

The effect of alloying elements on the corrosion resistance of rapidly solidified (RS) magnesium alloys was investigated. This was accomplished using electrochemical and gravimetric techniques in conjunction with scanning electron microscopy. Melt-spun ribbons were examined in 0.05M sodium borate (pH 9.2) and 0.025M sodium carbonate/0.025M sodium bicarbonate (pH 10.0) buffer solutions. Corrosion rates calculated from electrochemical impedance spectroscopy (EIS) and linear polarization data demonstrated that binary Mg-Al alloys with 15-45 wt.% Al possess excellent corrosion resistance. With Al as the primary alloying element (3-8 wt.%), corrosion rates of multicomponent alloys were measured using EIS. Results indicate that beneficial alloying elements include cerium (4-10 wt.%), manganese (0.4-3 wt.%), neodymium (5 wt.%), and yttrium (7 wt.%). Scanning electron microscopy showed that the RS alloys were attacked uniformly at relatively low rates, while pure magnesium in cast form suffered severe attack.

Advances in Magnesium Alloys and Composites
Edited by H. Paris and W.H. Hunt
The Minerals, Metals, & Materials Society, 1988

Introduction

The need for fuel efficiency and increased performance in aerospace systems necessitates continuous improvement of the properties of the materials used. Magnesium alloys are an exciting alternative to the aluminum alloys currently dominating this industry, due mainly to their low densities and potentially high strength/weight ratios. Rapid solidification processing (RSP), which has been used to improve the properties of several alloy systems (1), is now under consideration as a means for making magnesium alloys more suitable for widespread use in aerospace applications. Magnesium usage has been limited in many applications due to shortcomings in both its mechanical and corrosion properties. The problem of poor corrosion resistance, especially pronounced in the presence of metallic impurities or aggressive electrolyte species (e.g. Cl^-), is a major obstacle to increased use of magnesium alloys.

Rapid solidification results in microstructural and chemical changes which often improve material properties, including strength, ductility, corrosion resistance, and thermal stability. While this paper focuses on the corrosion behavior of RS Mg alloys, recent review articles include more thorough discussions of the use of RSP to improve the properties of Mg alloys (2,3). With respect to corrosion resistance, rapid solidification shows promise as a means for making magnesium alloys better-suited for applications such as aerospace structural components. Chang et al. utilized rapid solidification and rare earth (RE) additions to develop Mg-Al-Zn alloys having very low corrosion rates in saltwater immersion tests (4), and Hagans described electrochemical studies showing improved passive film stability for $Mg_{70}Zn_{30}$ metallic glass (5). These improvements are a function of the type and concentration of alloying elements, and this work seeks to provide a better understanding of the role played by alloying elements in the corrosion behavior of these relatively new materials.

Experimental work focused on using electrochemical techniques to determine the effect of various alloying elements on the corrosion rates of binary and multicomponent RS Mg alloys produced by melt-spinning. This processing route was selected because of the chemical and microstructural homogeneity which these ribbons tend to possess. The ribbons are small and fragile, however, and they are therefore not suitable for evaluation using the traditional weight-loss techniques, such as immersion or salt-spray tests. Electrochemical techniques were chosen for this study because they can be applied with relative ease to specimens in ribbon form, they allow faster determination of corrosion rates than the traditional techniques, and they may provide information on the electrical properties of the film on the alloy surface and the electrochemical mechanisms controlling the corrosion process.

Electrochemical impedance spectroscopy (EIS) was used to evaluate a large number of binary and multicomponent alloys in order to determine the additions most likely to result in improved corrosion resistance. A significant goal of this work was to establish a correlation between the corrosion rates

calculated using electrochemical techniques and those calculated from weight loss. This information was then combined with that from the mechanical and thermal studies to select a small number of multicomponent alloys for an extensive fundamental examination. Also reported here are the results of anodic polarization scans used to compare the protective ability of the passive films formed on alloy AZ61 (Mg-6Al-1Zn) in the cast and melt-spun condition. Finally, scanning electron microscopy (SEM) provided additional insights into the corrosion processes occurring on several cast and RS alloys.

Lockheed Missles and Space Company is currently conducting an extensive study whose goal is the selection of alloying elements which optimize overall performance. The selection process therefore includes examinations of mechanical properties, corrosion resistance, and thermal stability, as well as the information available in the literature. For this reason, and because of the limited reproducibility of the corrosion data, the selection of alloying elements for further study does not necessarily reflect the corrosion rates determined using EIS and presented here.

Experimental

Nearly all of the rapidly solidified alloys studied were in the form of melt-spun ribbons 1-3 mm wide and roughly 20-70 μm thick. The alloys were prepared from high-purity elements at the Lockheed Palo Alto Research Laboratory and melt-spun to ribbon form at the National Bureau of Standards. Samples of alloys in their as-cast form were used for gravimetric studies and for determining effects of rapid solidification. Table I lists the binary and multicomponent RS alloys examined, with compositions given in weight percent.

Table I. RS Alloys Examined in This Study.

Binary Alloys	Multicomponent Alloys
Mg-4.8Zn	Mg-4.9Al-4.9Ce
Mg-18.6Zn	Mg-5.0Al-2.1Zn-5.9Ce
Mg-27.5Zn	Mg-5.4Al-3.6Li-5.7Ce
Mg-14.4Al	Mg-3.4Al-1.6Zn-7.1Y
Mg-28.8Al	Mg-4.5Al-1.6Zn-5.4Nd
Mg-42.8Al	Mg-4.8Al-1.0Mn-2.0Zn-7.0Ce
Mg-2.0Li	Mg-5.0Al-1.7Li-2.1Zn-3.3Ce
Mg-7.7Li	Mg-4.4Al-3.5Li-2.2Zn-5.2Ce
Mg-14.0Li	Mg-3.7Al-0.6Mn-2.2Zn-0.5Ca
Mg-5.5Ca	Mg-7.7Al-3.0Mn-1.8Zn-13.7Ce
Mg-11.3Ca	Mg-4.3Al-3.7Li-1.1Mn
Mg-1.7Si	Mg-3.1Al-3.1Li-0.4Mn-6.9Ce
	Mg-7.6Al-3.7Li-2.0Mn-1.8Zn-8.6Ce
	Mg-6Al-1Zn (Commercial Alloy AZ61)

*Compositions are given in weight percent.

Three types of electrochemical experiments were conducted: electrochemical impedance spectroscopy, linear polarization near the corrosion potential (E_{OC} or E_{corr}), and potentiodynamic anodic polarization. The experimental cell was made of polycarbonate and contained 1.5-2.0 liters of electrolyte. All experiments were conducted at room temperature (about 25°C) without stirring or deaeration. Two graphite rod counter electrodes were placed opposite the sample, which served as the working electrode, and a saturated calomel electrode (SCE) was used as the reference. Reagent-grade chemicals were used to make the two electrolytes: 0.05M sodium borate (pH 9.2) and 0.025M sodium carbonate/0.025M sodium bicarbonate (pH 10.0). The borate electrolyte was chosen so that results could be compared with previous studies on magnesium-base materials (5,6). The carbonate buffer was selected for some of the polarization studies in order to examine the effects of a more alkaline electrolyte on passivity. When added, chloride ion was introduced in the form of sodium chloride at levels of 100 ppm, 1000 ppm, or 3.5 wt.%.

Automated impedance measurements were made using either the PAR 368 or 378 Electrochemical Impedance Measurement System. These consist of a potentiostat/galvanostat, lock-in analyzer, and personal computer. Impedance spectra were generated over the frequency range of 5 mHz to 100 kHz using a 10 mV peak-to-peak AC perturbation. Varying the amplitude of this perturbation between 5 and 20 mV caused almost no change in the frequency response of the Mg/borate system. A dummy cell, consisting of a resistor in series with a resistor/capacitor parallel combination, was used to check the accuracy of both measurement systems. Measurements were started after E_{OC} stablilized, usually about 60-90 minutes after immersion. Corrosion rates determined using EIS are based on experiments conducted with E_{OC} as the DC potential.

Linear polarization measurements were conducted following the guidelines in ASTM G 59. Automated measurements were made using a computer-controlled potentiostat. In general, the response was linear over a range of about ±15-20 mV vs. E_{OC}, and this was confirmed for each set of data before making calculations. To compensate for ohmic drop in the electrolyte, either a current-interrupt feature of the measurement circuit was used or the electrolyte resistance was determined using EIS and then subtracted.

Anodic polarization scans were generated at 0.1 or 0.2 mV/s using either manual or automated potentiodynamic systems. Compensation for potential drop in the electrolyte was accomplished as described for linear polarization measurements. Scans were started at E_{corr} after a steady-state value was established, usually in 60-90 minutes. These scans were continued until transpassivity was observed, or in the case of chloride additions, until pit propagation was clearly observed.

Results are reported only for the free (non-contact) side of the melt-spun ribbon specimens, because this side possessed greater chemical homogeneity and less likelihood of contamination from the wheel than the contact surface. Note, however, that little difference in general corrosion resistance was observed for the specimens whose contact surface was examined. Ribbon samples were mounted in a room-temperature epoxy potting compound by laying the ribbon, non-contact side

facing out, on the partially-cured epoxy. After the epoxy was completely hardened, an insulated wire was attached using silver paint, and this contact was then covered with more epoxy to leave a nearly two-dimensional alloy surface exposed. A similar procedure was used for mounting the as-cast samples. All electrode areas were measured to the nearest 0.01 cm^2. RS ribbon electrodes were rinsed in acetone and deionized water before immersion in the cell; cast alloy samples were polished to 600-grit SiC before rinsing in acetone and deionized water.

Gravimetric studies were carried out on several of the cast alloys and on pure Mg as a means of establishing the accuracy of electrochemical corrosion-rate measurements. Samples for gravimetric studies were prepared by polishing a cube of the material to 400-grit SiC, measuring the surface area to 0.01 cm^2, and then polishing to 600-grit. After rinsing the samples in acetone and drying them in a stream of warm air, they were weighed to the nearest 1 mg, rinsed in deionized water, and placed in the electrolyte. Upon removal after 4-8 days immersion, the samples were cleaned according to ASTM G 1 in hot 20% chromic acid containing about 1% silver nitrate or silver chromate. They were then rinsed in deionized water and acetone before final weighing.

Results and Discussion

Basis for Calculating Uniform Corrosion Rate

Weight-loss studies were conducted on several bulk alloy samples in order to assess the accuracy of corrosion rates determined using EIS and linear polarization. The measured weight loss was used to calculate a uniform penetration rate according to ASTM Standard G 1. The results of this comparison between gravimetric and electrochemical corrosion-rate measurements will be presented following a brief discussion of the latter.

Corrosion rates were calculated from electrochemical data, using either the EIS or linear polarization, by determining the polarization resistance, R_p. R_p, when normalized for area, is inversely proportional to the corrosion rate. For the case of linear polarization, R_p is measured as the slope of the potential-current density curve at the corrosion potential. This procedure is described in ASTM Standard G 59. After R_p is determined, the corrosion current density is calculated from the Stern-Geary relationship (7),

$$i_{corr} = \frac{b_a b_c}{2.3(b_a + b_c)R_p} \qquad (1)$$

where b_a and b_c are the anodic and cathodic Tafel constants, respectively. Typical values for b_a and b_c are 60 and 120 mV/decade, and these were the values assumed here. Values of b_c are fairly well established for hydrogen evolution, but not as well known for other reactions. Anodic polarization experiments provided a rough estimate of b_a as 60-80 mV for

magnesium dissolution. Note that Eqn. 1 is more sensitive to R_p changes than it is to changes in b values. The penetration rate in mils per year (mpy) was then calculated based on Faraday's law. The above form of the Stern-Geary equation shows that R_p has the unique units of ohms-cm^2. This means that for typical impedance data in ohms, the Stern-Geary relationship yields a current, rather than current density, which must then be divided by the electrode area in order to calculate a corrosion rate.

Since a complete discussion of the application of EIS to corrosion studies is beyond the scope of this paper, its use in calculating the uniform corrosion rates presented here will be described only briefly. The reader is referred to the literature for more thorough treatments (8,9,10). Based on some previous EIS studies on magnesium (6,11), a Randles circuit (12) was chosen as an equivalent circuit for modelling the corrosion process on magnesium alloys. Equivalent circuit models do not describe the physical processes occurring on an electrode surface; however, they often facilitate the measurement of certain parameters, such as R_p. The Randles circuit is the simplest and most commonly-used equivalent circuit, consisting of a single RC parallel combination in series with the electrolyte resistance (R_s). The resistance within the RC combination represents R_p and the capacitance C_{dl}, the double-layer capacitance due to charge separation at the interface.

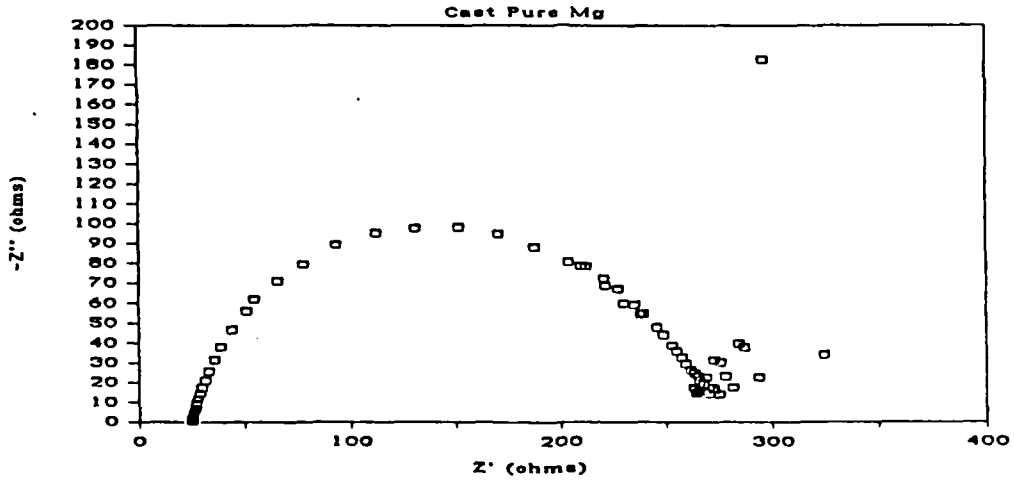

Figure 1 - Nyquist presentation of EIS data for cast pure Mg in pH 9.2 Na borate.

Figure 1 shows EIS data for pure Mg in pH 9.2 sodium borate presented in the complex plane, or Nyquist, format. This format plots the negative imaginary component of the impedance, -Z'', against the real component, Z', with frequency (increasing from right to left) as a parameter on the plot. Except at very low frequencies, the data is typical of simple Randles-circuit behavior, showing a capacitive semicircle with real-axis intercepts equal to R_s and R_s+R_p at high and low frequencies, respectively. Semicircles fitted to the Nyquist

plots were nearly always depressed up to about 20°, and the depressed diameter was used for determining R_s and R_p. The goal of the bulk-alloy studies was to establish a correlation between the corrosion rate calculated using this primary capacitive loop and that measured from weight loss. An interpretation of the entire frequency response is a future goal of this study. This is an important goal because the impedance data for several of the alloys was more complex than that shown in Figure 1, involving another time constant at low frequency.

Correlating Weight-Loss and EIS Measurements

Figure 2 compares the results of penetration rates in 0.05M Na borate (pH 9.2) calculated from EIS, linear polarization, and gravimetric analysis. The Mg-Al-Zn-RE alloys are bulk alloys whose compositions are proprietary. As these results indicate, the electrochemical techniques measured the uniform corrosion rates of these materials relatively accurately, except for the pure magnesium, which had a weight loss roughly an order of magnitude higher than that predicted by EIS or linear polarization. Similar results have been previously reported for magnesium (13,14,15), and in those cases the authors attributed this "negative difference" to either an anomalous valence effect due to the existence of univalent Mg, or a "chunk" effect involving the removal of small particles by an undermining action. This is believed to occur because the particle, for example an iron-rich impurity phase, is cathodic to the surrounding Mg matrix, which corrodes at this particle boundary by galvanic action. The particle subsequently falls out, resulting in a mass loss much higher than that due only to the dissolution that is measured using EIS and linear polarization. Based on the large difference observed, it was assumed in this work that the cause was the chunk effect. Scanning electron microscopy was used to examine the samples closely after immersion as a means of checking for evidence of this phenomenon (Figures 3-5).

Corrosion of the pure magnesium was non-uniform, having an etched appearance when viewed with the naked eye or under low magnification with an optical microscope. Scanning electron microscopy was then used to examine these surfaces more closely. Figure 3 is an SEM photomicrograph showing a pure Mg surface after a 7-day immersion in pH 9.2 sodium borate, followed by removal of the corrosion products. Present in this micrograph is particle, roughly 10 μm in diameter, which has been partially undermined by dissolution of the surrounding matrix. Such particles were widely distributed over the surfaces of all of the pure Mg samples examined, whether or not Cl^- had been present during the immersion. In contrast, the surface of cast AZ61 is shown in Figure 4 after a 7-day immersión in the same borate buffer. This relatively uniform attack is representative of the cast alloys which had corrosion rates that were accurately measured using EIS (Figure 2).

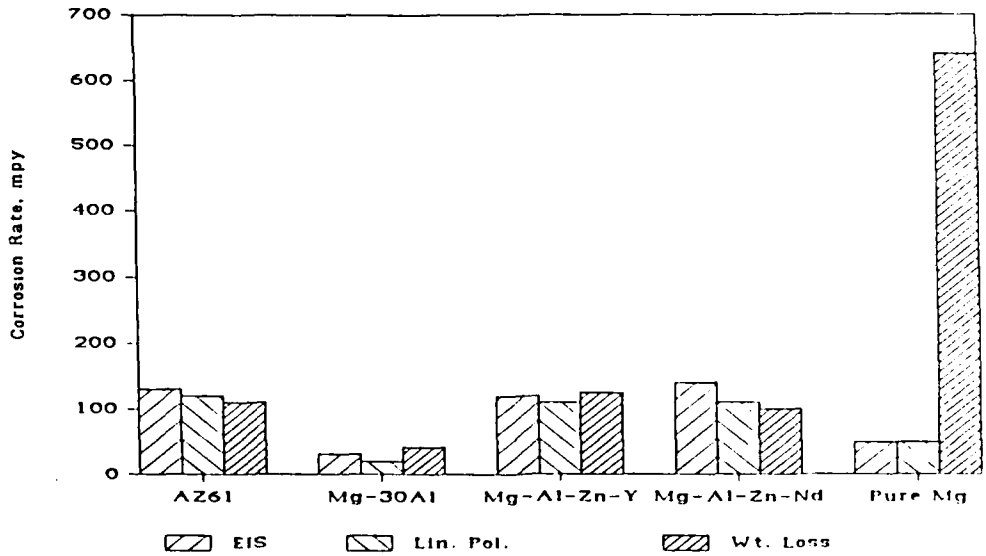

Figure 2 - Comparison of corrosion rates of bulk alloys in pH 9.2 Na borate calculated from electrochemical and gravimetric techniques. The exact compositions of the Mg-Al-Zn-RE alloys are proprietary.

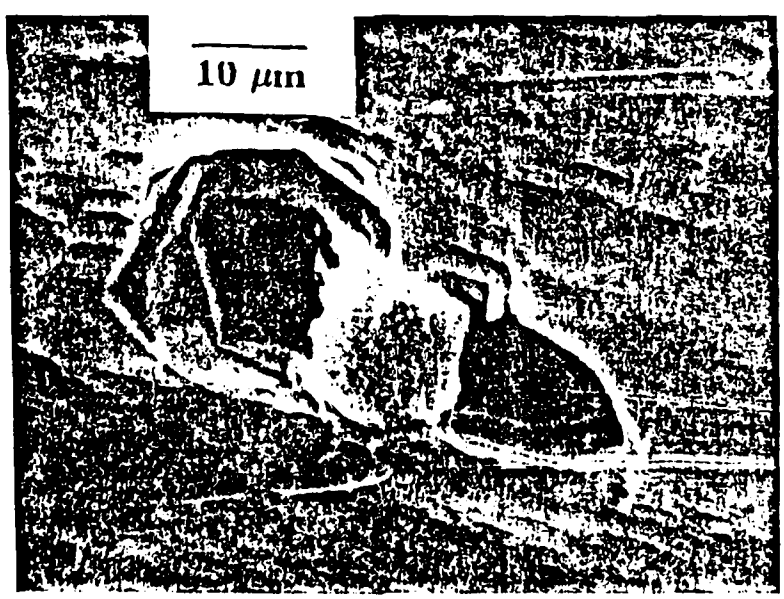

Figure 3 - SEM photomicrograph of pure Mg surface after one-week immersion in pH 9.2 Na borate and subsequent removal of corrosion products.

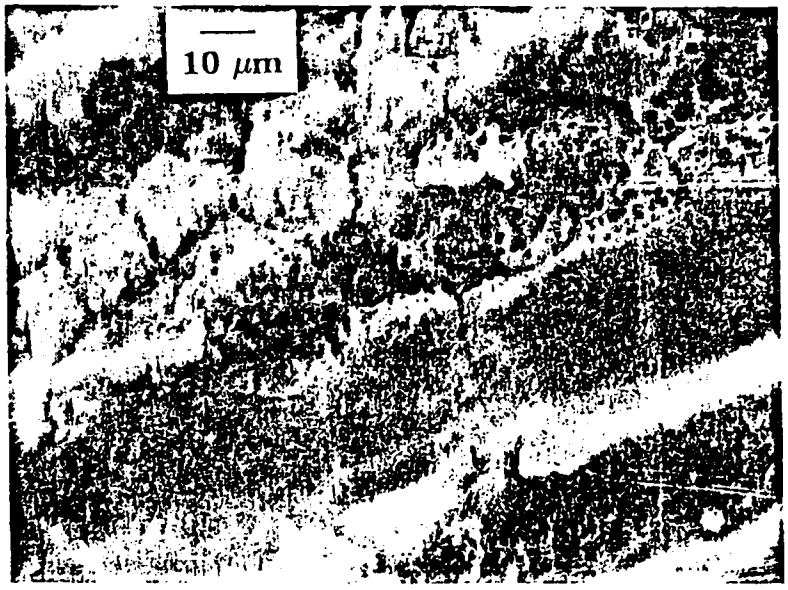

Figure 4 - SEM photomicrograph of cast AZ61 surface after one-week immersion in pH 9.2 Na borate and subsequent removal of corrosion products.

While generating impedance spectra or linear polarization data, RS ribbon samples were exposed to the electrolyte for up to several hours, and the corrosion products were then removed. In general, the RS alloys were attacked even more uniformly than the bulk alloys, and the RS Mg-14.4Al surface shown in Figure 5 is typical of the ribbons examined. Since this uniform attack was observed on nearly all of the ribbons examined, the electrochemical techniques were considered adequate for measuring the uniform corrosion rates reported. The corrosion rate of RS samples of pure Mg measured by EIS was nearly the same as that measured for the cast Mg, but the attack was very uniform on the RS Mg. This implies that EIS provided an accurate measure of the instantaneous corrosion rate of the cast Mg, and provides a basis for using pure Mg as a baseline in evaluating the effects of alloying elements.

This is a useful finding because such a correlation has not been previously reported for magnesium-base materials. This correlation might be strengthened by determining how representative the electrochemical data are of steady-state conditions. Since the ribbon samples used in the electrochemical studies were immersed for only a few hours, the transient behavior of weight loss and the electrochemically-determined R_p will be examined in future studies. R_p vs. time behavior, examined for cast Mg in sodium borate/3.5% NaCl using EIS, indicated a decrease in R_p of about 25% in the first 5 days, but little change afterwards. However, rather than an increase in the corrosion rate, this decrease in R_p may be caused mostly by an increase in surface area resulting from the non-uniform attack of pure Mg discussed earlier. A bulk Mg-Al-Zn-Nd alloy, similar in composition to

the one listed in Table I, was immersed for two weeks in unbuffered 3% NaCl while generating electrochemical impedance spectra periodically. Like the other alloys, this material was attacked uniformly, and R_p changes indicated a decrease in the corrosion rate with time. This decrease was probably due to an increase in pH at the electrode surface to a value where thermodynamics predicts that a stable oxide or hydroxide film forms on Mg.

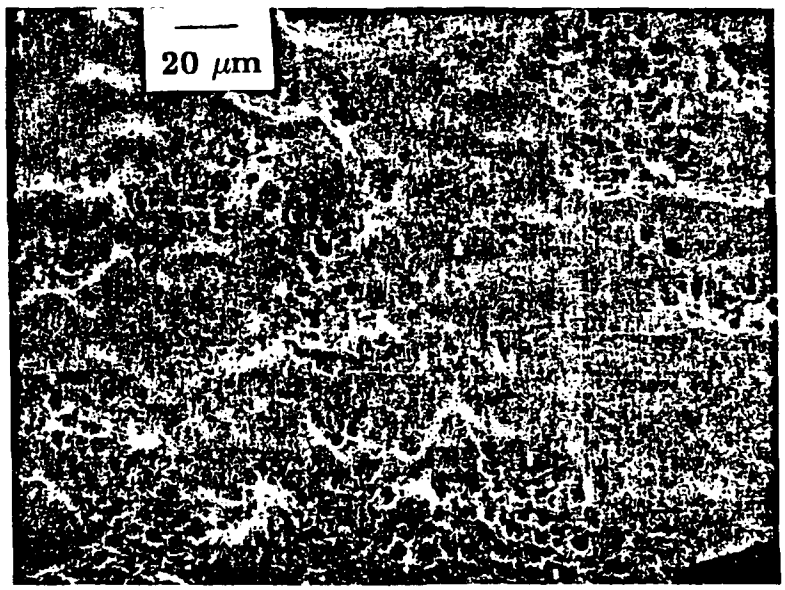

Figure 5 - SEM photomicrograph of RS Mg-14.4Al ribbon after EIS examination in pH 9.2 Na borate and subsequent removal of corrosion products.

Corrosion Rates of RS Magnesium Alloys

The corrosion rates of the binary and multicomponent alloys (Table I) in pH 9.2 sodium borate were measured using EIS. Although alloy design is not the purpose of this study, some discussion of the alloying-element selection process is necessary since it includes more than just the corrosion behavior. In addition to corrosion rate, evaluation of alloying elements also includes their mechanical and thermal properties.

Figure 6 summarizes the corrosion-rates of the binary RS alloys, measured in pH 9.2 sodium borate using EIS. Aluminum is the only element which improved the corrosion resistance, causing the rate to decrease as Al content increased. Surface analyses indicated that the air-formed oxide on the Mg-Al alloys was a layered structure composed of MgO/Mg-Al-oxide/substrate, with the oxide (Mg-rich) thinner with increasing Al content. This benefit of aluminum is likely related to the nature of this oxide, the strong tendency for Al

to form a stable passive film in this electrolyte, and the lack of galvanic action between Mg and Al in these alloys. These results also show that small additions of lithium do not seriously degrade the corrosion resistance of pure magnesium. Lithium was examined mainly because of its very low density. Small amounts of Li added to magnesium caused only a slight increase in the corrosion rate compared to Zn, Ca, and Si, suggesting that lithium additions of about 2 wt.% are not undesirable.

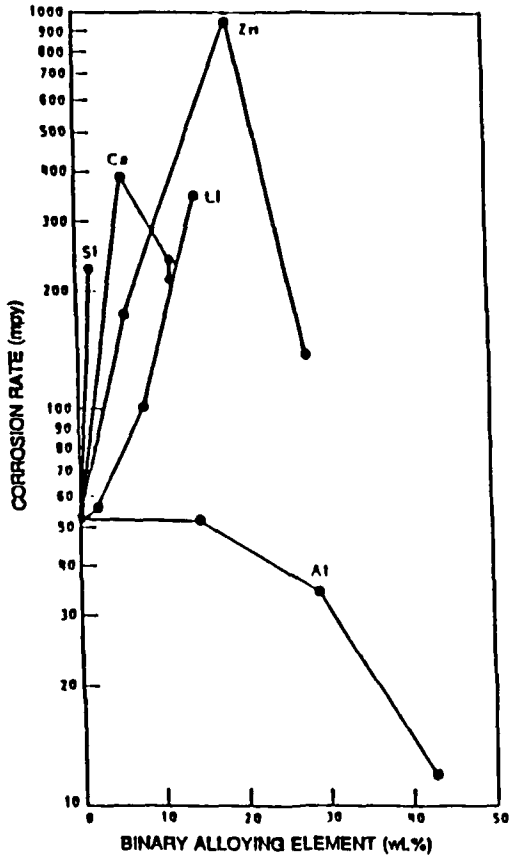

Figure 6 - Corrosion rates of binary RS magnesium alloys determined using EIS.

Zinc had a somewhat anomalous effect on the corrosion behavior of Mg, as evidenced by the peak seen in Fig. 6 at the 18.6 wt.% level. This intermediate addition caused a drastic increase in the corrosion rate, while additions of 4.8 % and 27.5 % had corrosion rates only slightly higher than that measured for pure Mg. Surface analysis indicated the presence of oxide films whose thickness decreased with increasing Zn content, none of which contained ZnO. More recent analysis found that the zinc content in the film increases with exposure time in the borate buffer. The 27.5 % Zn content is still lower than that required for glass formation (42-65 wt.% Zn), so the role of zinc at high levels is unclear and warrants further study. For alloys of practical interest to this study, the Zn content must be small due to its high density, and these corrosion data suggest that low zinc levels are not as harmful as those of silicon and calcium. However, calcium enhances the

oxidation resistance of molten magnesium and the atmospheric oxidation of cast magnesium in moist air (16). An alloy containing 0.8 wt.% Ca was therefore included in the multicomponent study in order to evaluate its effects on strength and corrosion resistance of a complex alloy.

Included in the multicomponent studies were some alloying elements not thoroughly examined in the binary studies. Manganese is added to many commercial alloys, particularly those of the AZ series, for improved corrosion resistance. These additions are generally less than 1 wt.% and are believed to serve a dual purpose (17). First, the manganese is believed to settle iron particles from the melt, thereby lowering the Fe content of the product. Second, Mn tends to surround iron particles in the solid, making them less effective as local cathodes. This commercial success, along with some limited studies of binary Mg-Mn alloys, was the basis for choosing Mn as a constituent of several multicomponent alloys. Rare earth additions were not examined in the binary studies, but have improved the properties of several complex alloys recently studied (6,18). These studies showed that additions of Y, Nd, and Ce improved the strength and corrosion resistance of Mg-Al-Zn alloys, without causing significant loss of ductility.

The corrosion rates of the multicomponent alloys, measured in the same manner as in the binary studies, are presented in Table II. Based on these studies and on surface analyses, some additional conclusions regarding alloying elements were drawn. Cerium may be a beneficial addition, as indicated by the corrosion rates measured for alloys 7, 13, and 14. These alloys had relatively high Ce contents and the lowest corrosion rates measured in this study. Measurements of the corrosion rates of alloys 5 and 6, containing Y and Nd, respectively, were not in agreement at the two laboratories involved in this study. The measurements made at Lockheed Missles & Space Co. suggest that alloys 5 and 6 have corrosion rates among the

Table II. Corrosion Rates of Multicomponent RS Mg Alloys.[1]

Composition (wt.%)	Alloy No.	Corr. Rate (mpy)
Mg-4.9Al-4.9Ce	2	140
Mg-5.0Al-2.1Zn-5.9Ce	3	120
Mg-5.4Al-3.6Li-5.0Ce	4	170
Mg-3.4Al-1.6Zn-7.1Y	5	170
Mg-4.5Al-1.6Zn-5.4Nd	6	100
Mg-4.8Al-1.0Mn-2.0Zn-7.0Ce	7	82
Mg-5.0Al-1.7Li-2.1Zn-3.3Ce	8	150
Mg-4.4Al-3.5Li-2.2Zn-5.2Ce	9	120
Mg-3.7Al-0.6Mn-2.2Zn-0.8Ca	10	150
Mg-7.7Al-3.0Mn-1.8Zn-4.4Ce	11	110
Mg-4.3Al-3.7Li-1.1Mn	12	110
Mg-3.1Al-3.1Li-0.4Mn-6.9Ce	13	64
Mg-7.6Al-3.7Li-2.0Mn-1.8Zn-8.6Ce	14	73

[1]Melt-spun ribbons in pH 9.2 Na borate. Compositions are given in weight percent.

lowest in this study, while they were ranked considerably poorer in the JHU results. This ranking varied somewhat from batch to batch, suggesting that variations in the production and handling of the ribbons may have a significant impact on their corrosion properties. The Lockheed results, along with the encouraging corrosion data (for an unbuffered H_2O/NaCl solution) reported by Das and Chang (6) and Chang et al.(18), suggest that Y and Nd are beneficial additions which should be examined further. Both weight loss and EIS experiments conducted at JHU confirmed the low corrosion rates reported by Das and Chang for these alloys in unbuffered chloride-containing solutions.

The results also suggest that manganese improves the corrosion resistance of the complex alloys examined. For example, comparison of the corrosion rates of alloys 3 and 7 implies that addition of 1 wt.% Mn caused roughly a 30% decrease in the corrosion rate measured using EIS. Statistical analysis provided additional support for this conclusion, and Mn additions in the 1 wt.% range will be included in the future complex alloys. The single alloy containing calcium, alloy 10, had one of the highest corrosion rates measured, an effect observed previously in the binary Mg-Ca alloys. Furthermore, the studies of mechanical properties indicated no significant strengthening by Ca, and it was therefore excluded from further examination.

Passivity Studies of Cast and RSP AZ61

The effect of RSP on alloy AZ61 (Mg-6Al-1Zn) was examined using anodic polarization scans in the presence of chloride. The electrolytes used were 0.05M Na borate (pH 9.2) and 0.025M Na carbonate/0.025M Na bicarbonate (pH 10.0) with 100 ppm, 1000

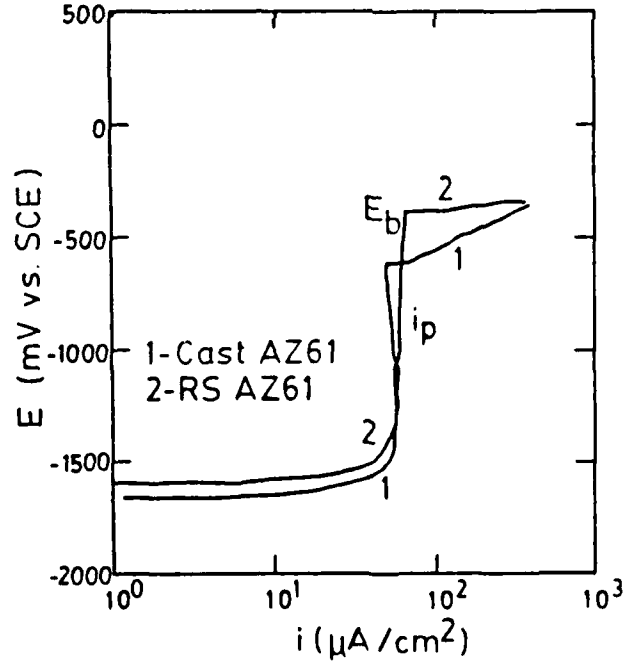

Figure 7 - Anodic polarization scans for cast and RS AZ61 in pH 10.0 Na carbonate/bicarbonate with 100 ppm NaCl.

ppm, or 3.5 % NaCl. Figure 7 presents anodic polarization data for cast and RS AZ61 ribbon in the carbonate buffer with 100 ppm NaCl. The characteristic parameters i_p and E_b are indicated. The passive current density, i_p, is an indication of the protective film's ability to maintain a low corrosion rate in the passive regime. The breakdown potential, E_b, is one measure of a metal's resistance to attack by an aggressive species; a higher (more positive) value of E_b indicates better resistance. E_b is a parameter which is dependent on experimental conditions, but is generally considered the potential at which the current begins to rise above its passive value due to breakdown of the film and subsequent pit propagation. Previous studies (19) revealed that i_p and open-circuit dissolution rate were affected little by RSP. However, some interesting improvements are seen in resistance to Cl^- attack.

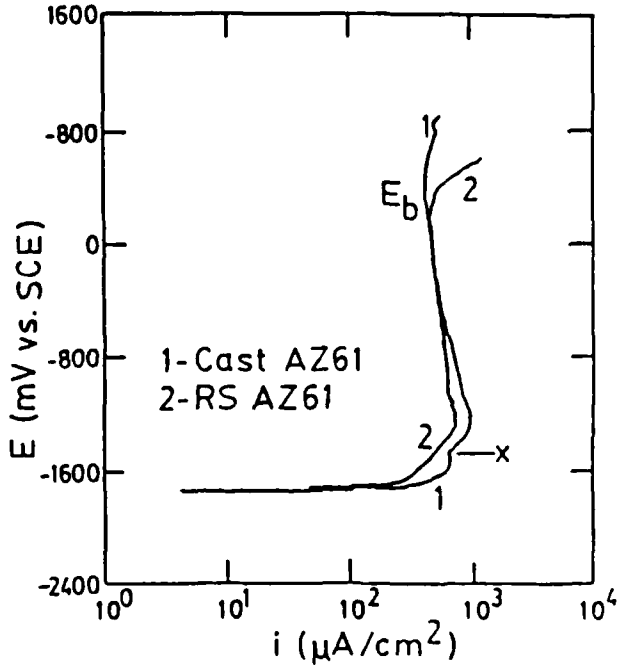

Figure 8 - Anodic polarization scans for cast and RS AZ61 in pH 9.2 Na borate with 100 ppm NaCl.

Figure 7 shows that the breakdown potential for the RS AZ61 is about 200 mV higher than that for the cast material. This 200 mV improvement was observed in the carbonate buffer at all Cl^- levels. Figure 8 presents the results of similar experiments conducted in the borate buffer with 100 ppm NaCl. The breakdown potentials do not indicate any improvement for the RS material, which was the case for all chloride levels. However, the current increase in the region marked "x" of the curve for the cast material at about -1.5 V (Figure 8) indicates pit initiation. These pits were also observed visually, and hydrogen evolved from them at a low rate during the remainder of the experiment. This event did not appear as a breakdown potential, probably due to the fact that the current involved in the slow propagation of these pits is not

large compared to i_p. The implication is that the borate-formed film more readily nucleates pits and is probably less stable on the cast AZ61. Figure 8 shows that the melt-spun alloy began pitting and the cast alloy developed new pits at about 400 mV, this value being slightly higher for the cast material.

These improvements may result from increased homogeneity or the formation of glassy films, possibly a combination of both. Similar results were found by Bertocci and Kruger, who used electrochemical noise studies to examine the passive films on Fe-Cr-Ni alloys (20). They showed that the film on a glassy alloy was more resistant to breakdown/repassivation events than that on its crystalline counterpart, but little change in overall current density was observed. Hagans recently studied $Mg_{70}Zn_{30}$ metallic glass and pure Mg in a pH 9.3 boric/borate buffer with 1000 ppm Cl^- (5). This alloy formed a more protective film than the pure metal, as reflected in a 400 mV improvement in the breakdown potential and a lower passive current density.

Conclusions

Several conclusions have been drawn from the work completed thus far in the study:

1. Corrosion rates of bulk Mg alloys calculated using EIS correlated well with those calculated from weight-loss data, as long as the attack was uniform. Uniform corrosion was observed on the RS Mg ribbons examined, strongly suggesting that EIS is a reliable method for evaluating the corrosion rates of the RS alloys.
2. Electrochemical corrosion-rate measurements of binary RS Mg ribbons showed aluminum to be the only element to cause a decrease in the corrosion rate of Mg. The corrosion rate decreased significantly as the Al content increased to 28.8 wt.% and above.
3. Additional elements found to be beneficial in small amounts include Ce and Mn. Complex alloys based on these additions maintained relatively low corrosion rates. Corrosion rates of the Nd- and Y-containing alloys examined in this study suggest that these two elements are detrimental. However, weight-loss and electrochemical studies using similar alloys (Mg-Al-Zn-RE alloys consolidated from RS particulate) in unbuffered 3% NaCl confirmed the beneficial effects of Nd and Y reported by other authors.
4. Anodic polarization studies of commercial alloy AZ61 indicated that the RS ribbon forms a more protective film than the cast material, especially in the carbonate buffer. This is likely due to the homogeneous character of the RS material, possibly combined with a tendency towards glassy-film formation.

Acknowledgements

The authors extend thanks to Professor Howard Jones of the University of Sheffield and Patrick Hagans of Dow Chemical Co. for their guidance in this work. We gratefully acknowledge Al Davinroy and Richard Lewis of Lockheed Missles & Space Co. for their guidance and preparation of alloys, and Robert Shull of the National Bureau of Standards for performing the melt-spinning. Thanks are also extended to Robert Kelly and Deniol Tanaka of The Johns Hopkins University for helpful discussions, and to Christopher Streinz and Thomas Mangiacapre of JHU for assisting in experimental work. This work was supported by the Air Force Wright Aeronautical Laboratories under Contract No. F33615-85-C-5032 and by the Air Force Office of Scientific Research under Contract No. F496620-86-C-0014. Sponsorship of the JHU Corrosion and Electrochemistry Research Laboratory by EG&G Princeton Applied Research is also acknowledged.

References

1. S. K. Das, K Okazaki, and C. M. Adam, "Applications of Rapid Solidification Processing to High Temperature Alloy Design," in High Temperature Alloys: Theory and Design, J. O. Steigler, ed. (Warrendale, PA: TMS-AIME, 1984), 451-471.
2. S. K. Das and C. F. Chang, "High Strength Magnesium Alloys by Rapid Solidification Processing," in Rapidly Solidified Crystalline Alloys, S. K. Das, B. H. Kear, and C. M. Adam, eds. (Warrendale, PA: TMS-AIME, 1985), 137-156.
3. H. Jones, A. Joshi, R. G. Rowe, and F. H. Froes, "The Current Status of Rapid Solidification of Magnesium-Base and Titanium-Base Alloys," The International Journal of Powder Metallurgy, 23 (1) (1987), 13-24.
4. C. F. Chang, S. K. Das, D. Raybould and A. Brown, "Corrosion Resistant High Strength Magnesium Alloys by RSP," Metal Powder Report, 41 (4) (1986), 302-308.
5. P. L. Hagans, "Electrochemical Study of the Passivation and Passive Film Breakdown of $Mg_{70}Zn_{30}$ Metallic Glass," Materials Research Society Symposium Proceedings, 80 (1987), 113-120.
6. P. L. Hagans, "AC Impedance Study of the Passivation of Mg, Al, and Mg Alloy AZ91B," Electrochemical Society Extended Abstracts, 83 (1) (1983), 112-113.
7. M. Stern and A. L. Geary, "Electrochemical Polarization," Journal of the Electrochemical Society, 104 (1) (1957), 56-63.
8. F. Mansfeld, "Recording and Analysis of AC Impedance Data For Corrosion Studies," Corrosion, 36 (5) (1981), 301-307.

9. D. D. Macdonald and M. C. H. Mckubre, "Electrochemical Impedance Techniques in Corrosion Science," in Electrochemical Corrosion Testing (ASTM STP 727), F. Mansfeld and U. Bertocci, eds. (Philadelphia, PA: ASTM, 1981), 110-149.

10. D. C. Silverman and J. E. Carrico, "Electrochemical Impedance Technique, a Practical Tool for Corrosion Prediction," (Paper No. 269, presented at the annual meeting of the National Association of Corrosion Engineers, San Francisco, CA, March 1987).

11. Private communication with P. Hagans, Dow Chemical Co., 1986.

12. J. E. B. Randles, "Kinetics of Rapid Electrode Reactions," Discussions of the Faraday Society, 1 (1947), 11-19.

13. R. L. Petty, W. Davidson, and J. Kleinberg, "The Anodic Oxidation of Magnesium Metal: Evidence for the Existence of Unipositive Magnesium," Journal of the American Chemical Society, 76 (1954), 363-366.

14. M. E. Straumanis and B. K. Bhatia, "Disintegration of Magnesium While Dissolving Anodically in Neutral and Acidic Solutions," Journal of the Electrochemical Society, 110 (5) (1963), 357-360.

15. W. J. James, M. E. Straumanis, B. K. Bhatia, and J. W. Johnson, "The Difference Effect on Magnesium Dissolving in Acids," Journal of the Electrochemical Society, 110 (11) (1963), 1117-1120.

16. E. F. Emley, Principles of Magnesium Technology (New York, NY: Pergamon Press, 1966).

17. H. A. Robinson and P. F. George, "Effect of Alloying and Impurity Elements in Magnesium Alloy Cast Anodes," Corrosion, 10 (6) (1954), 182-188.

18. C. F. Chang, S. K. Das, and D. Raybould, "Rapidly Solidified Mg-Al-Zn-Rare Earth Alloys," in Rapidly Solidified Materials (Metals Park, OH: ASM, 1986), 129-135.

19. J. Kruger, G. G. Long, and D. K. Tanaka, "A Fundamental Understanding of the Effect of Alloying Elements on the Corrosion Resistance of Rapidly Solidified Magnesium Alloys," First Annual Report to the Air Force Office of Scientific Research, The Johns Hopkins University, November 1986.

20. U. Bertocci and J. Kruger, "Studies of Passive Film Breakdown by Detection and Analysis of Electrochemical Noise," Surface Science, 101 (1980), 608-618.

SECTION IV

Corrosion Studies of Rapidly Solidified Magnesium Alloys

G.L. Makar and J. Kruger

Corrosion and Electrochemistry Research Laboratory

Department of Materials Science and Engineering

The Johns Hopkins University, Baltimore, Maryland 21218

Abstract

Effects of alloying elements on the corrosion resistance of mostly binary rapidly solidified (RS) magnesium alloys were examined using electrochemical techniques. Uniform corrosion rates were measured at room temperature in a pH 9.2 sodium borate buffer using electrochemical impedance spectroscopy (EIS). Comparisons of electrochemically and gravimetrically determined corrosion rates of bulk magnesium and magnesium alloys showed that the charge-transfer resistance could be used to accurately measure the corrosion rates of these materials provided the attack was indeed uniform. The correlation broke down for pure magnesium, which suffered a non-uniform attack due to the undermining of small particles. Corrosion-rate measurements of binary alloys showed that aluminum was the only element which caused a decrease in the corrosion rate of magnesium; the corrosion rate decreased with increasing aluminum content. Low concentrations of zinc and lithium resulted in alloys with corrosion rates slightly higher than that of the pure magnesium. Anodic polarization scans were used to compare as-cast and rapidly solidified commercial ternary alloy AZ61 in borate (pH 9.2) and carbonate/bicarbonate (pH 10.0) buffer solutions containing 100 ppm, 1000 ppm, and 3.5 wt.% sodium chloride. The RS AZ61 formed a more protective film than the cast material under these conditions.

Introduction

Magnesium alloys are a promising complement to the aluminum alloys currently dominating the aerospace industry, due mainly to their low densities and potentially high strength/weight ratios. The 1.74 specific gravity of magnesium is 35% lower than that of aluminum, and typical magnesium alloys weigh roughly 25% less than comparable aluminum alloys. Use of magnesium in structural aerospace applications exists, but has been limited due to shortcomings of both its mechanical and corrosion properties. The inherent low strength of many magnesium alloys is a significant factor, but the problem of poor corrosion resistance affects the viability of increased magnesium usage enough that the aerospace industry will probably reject new alloys offering better mechanical properties without improved corrosion resistance.

Magnesium is the most active metal used in engineering applications (1), and corrodes so readily in some environments that magnesium alloys commonly serve as sacrificial anodes. Despite this problem, magnesium alloys often perform well even in aqueous environments as long as the proper alloys and/or surface treatments are selected. Magnesium dissolution in aqueous environments generally proceeds by electrochemical reaction with water to produce magnesium hydroxide and gaseous hydrogen, a mechanism which is highly insensitive to the oxygen concentration (1). Reaction 1 describes the probable overall reaction in neutral and alkaline solutions.

$$Mg + 2H_2O \rightarrow Mg(OH)_2 + H_2 \quad (1)$$

This net reaction may be expressed as the sum of the following partial reactions:

$$Mg \rightarrow Mg^{2+} + 2e^- \quad (2)$$

$$2H_2O + 2e^- \rightarrow H_2 + 2(OH)^- \quad (3)$$

$$Mg^{2+} + 2(OH)^- \rightarrow Mg(OH)_2 \quad (4)$$

The mechanism described above probably involves some intermediate steps, most notably the initial production of monovalent magnesium ions having short lifetimes (2). Several studies of the kinetics of reaction 1 concluded that the acid-type attack which occurs at pH less than about 11 is controlled by diffusion of reactants or products through the surface film, even under open-circuit conditions (eg. 3,4,5). Results of more recent studies in solutions buffered at pH 9-10 favor a dissolution rate controlled by charge transfer at the corrosion potential and by diffusion where stable films would be expected to form (eg. at potentials in the passive regime) (6,7). As corrosion proceeds, the metal surface experiences a local pH increase due to the formation of $Mg(OH)_2$, whose equilibrium pH is approximately 11. The protection supplied by this film is therefore highly dependent upon the conditions of exposure. For example, magnesium is resistant to corrosion in small volumes of water which are free of species aggressive to the film.

There are two primary reasons for the poor corrosion resistance of many magnesium alloys: susceptibility to internal galvanic attack caused by alloying or impurity elements and conditions which hinder the stability of the protective film. In an extensive study of saltwater corrosion of magnesium and magnesium alloys, Hanawalt and co-workers quantified the sensitivity of magnesium to common impurity and alloying elements (8). They identified well-defined impurity concentrations, above which the corrosion rate of magnesium increased dramatically. The value determined for iron in high-purity magnesium (~99.994%), for instance, was 170 ppm. These tolerance limits can vary according to the phases in which the impurity elements exist and the concentration of other impurities or alloying elements (8,9). The "quasi-passive" hydroxide film on magnesium is much less stable than the truly passive film which can form on metals such as iron. For example, triply distilled magnesium in pH 9.3 sodium

borate/boric acid has a passive current density in the 1-2 mA/cm^2 range (10). Iron, on the other hand, has a passive current density of about $4 \mu A/cm^2$ in a similar electrolyte (11). Another characteristic of this quasi-passivity is the poor pitting resistance of magnesium and its alloys.

Rapid solidification processing (RSP) is a method of altering the phase constituency and microstructure of a material through systematic quenching at rates of 10^5-10^7 °C/s, several orders of magnitude faster than typical rates for conventional processing routes. Specific microstructural modifications include extended solid solubility, increased chemical homogeneity, and possible glass formation. Improvements in several properties of magnesium alloys due to rapid solidification have been studied and described recently (eg. 10,12,13,14), but the present discussion focuses solely on corrosion resistance. Chang et al. utilized rapid solidification and rare earth (RE) additions to develop Mg-Al-Zn-RE alloys having low corrosion rates in saltwater immersion tests (14), while Hagans described electrochemical studies showing improved passive film stability for $Mg_{70}Zn_{30}$ metallic glass (10). These improvements are a function of the type and concentration of alloying elements, and this work seeks to provide a better understanding of the role played by alloying elements in the corrosion behavior of these relatively new materials. The results described here represent the first steps toward that goal.

Experimental work focused on using electrochemical techniques to determine the effect of various alloying elements and their concentration on the corrosion rates of binary RS Mg alloys produced by melt-spinning. This processing route was selected because of the chemical and microstructural homogeneity which these ribbons tend to possess. The ribbons are small and fragile, however, and hence difficult to evaluate using the traditional weight-loss techniques, such as immersion or salt-spray tests. Electrochemical impedance spectroscopy (EIS) was selected to evaluate the alloys, and a significant objective of this work was to establish a correlation between the corrosion rates calculated using electrochemical techniques and those calculated from weight loss of bulk specimens. Also reported here are the results of anodic polarization scans used to compare the protective ability of the passive films formed on alloy AZ61 (Mg-6Al-1Zn) in the cast and melt-spun condition. Finally, scanning electron microscopy (SEM) provided additional insights into the corrosion processes occurring on several cast and RS alloys.

Experimental

Nearly all the rapidly solidified alloys studied were in the form of melt-spun ribbons 1-3 mm wide and 20-70 μm thick. The alloys were prepared from high-purity (at least 99.9%) elements at the Lockheed Palo Alto Research Laboratory (LPARL) and melt-spun to ribbon form at the National Bureau of Standards (now the National Institute for Standards and Technology.) Samples of pure Mg (99.98%) and Mg-base alloys, including one binary and three multicomponent alloys, were examined in the as-cast form in order to compare gravimetric and electrochemical

measurements. Commercial alloy AZ61 (Mg-6Al-1Zn) was examined in both cast and ribbon form to determine effects of rapid solidification. The cast AZ61 had an average grain size of about 40 μm, with precipitates concentrated in, but not limited to, grain boundaries and adjacent regions. $Mg_{17}Al_{12}$ was identified by LPARL as the principal second phase in the Al-containing alloys. This phase is expected in magnesium alloys with more than about 2 wt.% aluminum. Table I presents the supplier's spectroscopic analysis of the magnesium used for experiments involving pure Mg and for producing alloys. Table II lists the binary RS alloys examined, with compositions given in weight percent. Optical metallography of the ribbons, including AZ61, revealed highly refined microstructures having equiaxed grains no more than a few μm in diameter; some had microstructures not resolved by optical techniques. Most of these solute-rich alloys contained additional phases which were distributed much more homogeneously than in their as-cast counterparts. The Mg-Ca, Mg-Li, and Mg-4.8Zn alloys were predominantly single-phase solid solutions.

Three types of electrochemical experiments were conducted: electrochemical impedance spectroscopy, linear polarization near the corrosion potential (E_{oc} or E_{corr}), and potentiodynamic anodic polarization. The experimental cell was made of polycarbonate and contained 1.5-2.0 liters of electrolyte. All experiments were conducted at room temperature (about 25 °C) without stirring or deaeration. Two high-density graphite rod counter electrodes were placed opposite the sample, which served as the working electrode, and a saturated calomel electrode (SCE) was used as the reference. Reagent-grade chemicals were used to make the two electrolytes: 0.05M sodium borate (pH 9.2) and 0.025M sodium carbonate/0.025M sodium bicarbonate (pH 10.0). The borate electrolyte was chosen so that results could be compared with previous studies of magnesium-base materials (7). The carbonate buffer was selected for some of the polarization studies in order to examine the effects of a more alkaline electrolyte on passivity. When added, chloride ion was introduced in the form of sodium chloride at levels of 100 ppm, 1000 ppm, or 3.5 wt.%.

The automated impedance measurement system consisted of a potentiostat/galvanostat and lock-in analyzer which were controlled by a personal computer. Impedance spectra were generated over the frequency range of 5 mHz to 100 kHz using a 10 mV peak-to-peak AC excitation. Varying the amplitude of this perturbation between 5 and 20 mV caused almost no change in the frequency response of the Mg/borate system. A dummy cell, comprised of a resistor in series with a resistor/capacitor parallel combination (RC-R), was used to check the accuracy of both measurement systems. Measurements were started after E_{oc} stablilized, usually about 60-90 minutes after immersion. Impedance spectra measured at E_{oc} typically showed the RC-R (Randles circuit) behavior characteristic of a single charge-transfer process, in which case the polarization resistance (R_p) was determined from the diameter of the semicircle formed by the data in the complex-plane (Nyquist) format. Corrosion current densities

were then calculated from the Stern-Geary relationship using anodic and cathodic Tafel constants of 60 mV (approximated from polarization data) and 120 mV (assumed), respectively. The treatment of more complex impedance spectra is discussed with the presentation of results.

Linear polarization measurements were conducted following the guidelines in ASTM G 59. Automated measurements were made using a computer-controlled potentiostat. In general, the response was linear over a range of about ±15-20 mV vs. E_{oc}, and this was confirmed for each set of data before making calculations. To compensate for ohmic drop in the electrolyte, either a current-interrupt feature of the measurement circuit was used or the electrolyte resistance was determined using EIS and then subtracted. Corrosion rates were calculated as described above for EIS procedures. Anodic polarization scans were generated at 0.1 or 0.2 mV/s using either manual or automated potentiodynamic systems. Compensation for potential drop in the electrolyte was accomplished as described for linear polarization measurements. Scans were started at E_{corr} after a steady-state value was established, usually in 60-90 minutes. These scans were continued until transpassivity was observed, or in the case of chloride additions, until pit propagation was clearly observed.

Results are reported only for the free (non-contact) side of the melt-spun ribbon specimens because this side possessed greater chemical homogeneity and less likelihood of contamination from the wheel than the contact surface. Note, however, that little change in general corrosion resistance was observed for the specimens whose contact surface was also examined. Ribbon samples were mounted in a room-temperature epoxy potting compound by laying the ribbon, non-contact side facing out, on the partially cured epoxy. After the epoxy was completely hardened, an insulated wire was attached using silver paint, and this contact was then covered with more epoxy to leave a nearly two-dimensional alloy surface exposed. A similar procedure was used for mounting the as-cast samples. All electrode areas were measured to the nearest 0.02 cm^2. RS ribbon electrodes were rinsed in acetone and deionized water before immersion in the cell; cast alloy samples were polished to 600-grit SiC before rinsing in acetone and deionized water.

The objective of the gravimetric studies was to establish the accuracy of electrochemical corrosion-rate measurements. Samples for gravimetric studies were prepared by polishing a cube of the metal or alloy to 400-grit SiC, measuring the surface area to 0.02 cm^2, and then polishing to 600-grit. After rinsing the samples in acetone and drying them in a stream of warm air, they were weighed to the nearest 1 mg, rinsed in deionized water, and placed in the electrolyte. Upon removal after 4-8 days immersion, the samples were cleaned according to ASTM G 1 in hot 20% chromic acid containing about 1% silver nitrate or silver chromate. They were then rinsed in deionized water and acetone before final weighing. Corrosion rates were calculated in mpy according to ASTM G1.

Results and Discussion

Correlating EIS and Gravimetric Corrosion-Rate Measurements - The goal of the weight-loss studies discussed here was to evaluate how successfully EIS was used to determine R_p values for calculating the corrosion rates of magnesium alloys in sodium borate. Five magnesium-base materials in bulk form were examined in these experiments: pure magnesium, commercial alloy AZ61, high-purity Mg-30Al, an Mg-Al-Zn-Y alloy (Allied Corp.), and an Mg-Al-Zn-Nd alloy (Allied Corp). These materials were all in the as-cast form, except for the Mg-Al-Zn-Nd alloy, which was extruded from crushed RS ribbon into bar form. Electrochemical impedance spectra, in both Nyquist and Bode formats, are shown for pure Mg, cast AZ61, and cast Mg-Al-Zn-Y in Figures 1-3. Figures 1 and 3 are representative of the impedance data for some of the alloys examined in this study, showing a single capacitive semicircle indicative of a charge-transfer process only. Note, however, that the low-frequency data for cast AZ61 (Figure 2) shows an additional time constant, the origin of which has not yet been identified. It appeared in the alloys high in aluminum, and was generally absent in those alloys having less than about 5% Al. This low-frequency behavior resembled a charge-transfer impedance in some cases and a diffusion impedance in others. The impedance behavior of these Al-containing alloys at low frequency may be related to the role of the surface film, which would be expected to gain significance as Al content increases.

Since the Randles circuit model does not apply to alloys with this additional time constant, a new approach was necessary for determining the corrosion rate based on the complex impedance behavior described above. In cases where corrosion is not controlled by one-step, Tafel behavior, charge-transfer reactions, the polarization resistance (the slope of the steady-state polarization curve at E_{oc}) may no longer serve as a measure of the corrosion rate. In many such cases (eg. diffusion control, multistep electron transfer), it is the charge-transfer resistance (R_{ct}) which may be used in a Stern-Geary expression to determine the corrosion rate (15). With respect to the frequency spectrum of AZ61 (Figure 2), R_{ct} corresponds to the diameter of the high-frequency capacitive semicircle. Therefore, all corrosion rates determined using EIS in this study were based on the diameter of the high-frequency capacitive semicircle. This corresponds to R_{ct} in all cases, and to R_p in those cases where the impedance spectrum collapses to RC-R behavior ($R_{ct} = R_p$). Figure 4 compares the corrosion rates measured in 0.05M Na borate (pH 9.2) using EIS, linear polarization, and gravimetric measurements. These results indicate that impedance spectroscopy measured the uniform corrosion rates of these materials relatively accurately, except for the pure magnesium, which had a weight loss roughly an order of magnitude higher than that predicted by EIS or linear polarization.

This lack of parity in the electrochemical and gravimetric results for pure Mg may be described as a "negative difference" effect which relates the observed corrosion rate upon application of an external current to the corrosion rate in the absence of external current (16). The following equation describes the theoretical relationship between these quantities:

$$I_{corr} + I_{app} - I_{obs} = 0 \qquad (5)$$

where:

I_{corr} = the corrosion rate at open circuit

I_{app} = the current applied to hold the specimen at some potential not equal to E_{oc}

I_{obs} = the observed corrosion rate when I_{app} is applied

Marsh and Schaschl found that for steel these components could sum to a number greater than zero (positive difference) or less than zero (negative difference). In this work, equation 5 reduces to a difference between I_{corr} and I_{obs}, since the experiments were conducted under open-circuit conditions ($I_{app}=0$). Since the weight loss (I_{obs}) was higher than the dissolution rate determined using electrochemical techniques (I_{corr}), Figure 4 indicates a negative difference for pure Mg. This phenomenon has been reported for magnesium dissolution in several previous studies (2,17,18,19).

Petty et al. attributed the discrepancy to the existence of univalent magnesium (19). This changes the corrosion rate calculated from electrochemical data because it changes the average valence used to convert corrosion current (i.e. charge passed) to a penetration rate. Petty and co-workers found that strong oxidizing agents (eg. MnO_4^-) caused less hydrogen evolution and the production of an additional reduction product at the Mg anode, but not at the Mg cathode. They determined the average valency in a number of aqueous electrolytes, with resultant values between 1.33 and 1.66. Hoey and Cohen examined magnesium anodes in various electrolytes, observing an acid type of attack at pH less than 10, resulting in an etched surface (2). They also measured low current efficiencies, attributing this effect to disintegration of the electrode into flakes which they saw fall to the bottom of the cell and evolve hydrogen. To examine this effect further, Straumanis and Bhatia studied the anodic dissolution of magnesium in neutral and acid solutions (17) and James et al. studied the dissolution of Mg in acids (18). In both cases, the authors attributed much of the negative difference to disintegration of the metal into fine particles, describing it as a "chunk" effect.

A knowledge of the role of impurtity elements in magnesium dissolution provides an understanding of the processes leading to the chunk effect. Particles which have low hydrogen overvoltage and electrode potentials significantly electropositive with respect to magnesium cause rapid dissolution of the surrounding matrix as they evolve gaseous hydrogen. In the studies by Straumanis et al. and James et al., average valencies were calculated in their efforts to explain the negative differences observed. Although univalent magnesium probably existed,

anomalous valence could not completely account for the difference because average values for the valence were unrealistically low ($n << 1$), as was the case in the present study. Considering the case of pure Mg in Figure 4, even if the metal dissolved exclusively as a univalent ion, a limiting value of $n = 1$ would merely double the corrosion rate calculated using EIS and linear polarization. The order of magnitude difference observed here would correspond to a mean valence of 0.2. For this reason, it was postulated that the negative difference seen in the data for pure Mg (Figure 4) was caused by the chunk effect. Recalling the sensitivity of magnesium to a variety of common impurities (8), such a mechanism seems likely since the magnesium used in this study contained significant concentrations of a variety of impurity elements (Table I). SEM was then used to check for evidence of this phenomenon.

Corrosion of the cast pure magnesium in sodium borate was non-uniform, having an etched appearance when viewed with the naked eye or at low magnification with an optical microscope. Hoey and Cohen described magnesium surfaces similarly etched in solutions of $pH < 10$ at room temperature (2). In the present work, this effect was observed after only 1-2 hours in the borate solution and was severe after one week. Electron microscopy allowed a closer inspection of this attack, as seen in the photomicrograph of Figure 5. Higher magnification was then used to determine if undermining of small particles contributed to this non-uniform attack. Figure 6 is an SEM photomicrograph showing a pure Mg surface after a 7-day immersion in pH 9.2 sodium borate followed by removal of the corrosion products. Visible in this photomicrograph is a particle, roughly 10 μm in diameter, which has been partially undermined by dissolution of the surrounding matrix. Such particles were distributed over the surface of all the pure Mg samples examined, whether or not Cl^- had been present during the immersion. In contrast, the surface of cast AZ61 is shown in Figure 7 and cast Mg-Al-Zn-Y in Figure 8 after immersion for about one week in 0.05M Na borate. This relatively uniform attack is representative of the materials whose corrosion rates were accurately measured using EIS (Figure 4).

As stated earlier, the RS ribbons were not evaluated using gravimetric corrosion-rate measurements. Although this precludes a direct evaluation of the accuracy of the electrochemical techniques for measuring the corrosion rates of the ribbons, SEM studies showed that they were, in general, attacked even more uniformly than the bulk alloys. Figure 9 is an SEM photomicrograph showing an RSP Mg-14.4Al electrode specimen after exposure to pH 9.2 sodium borate. Based on the bulk alloy studies discussed above, the uniform attack of the ribbon alloys, represented by Figure 9, implies that the corrosion rates of the RS ribbons were accurately determined using EIS. This correlation might be strengthened by determining how representative the electrochemical data are of steady-state conditions. Since the ribbon samples used in the electrochemical studies were immersed for only a few hours, the time dependence of weight loss and the electrochemically determined R_p should be examined in future studies. R_p vs. time behavior, examined for cast Mg in sodium borate/3.5% NaCl using EIS, indicated a

decrease in R_p of about 25% in the first 5 days, but little change afterwards. However, rather than an increase in the corrosion rate, this decrease in R_p may be caused mostly by an increase in surface area resulting from the non-uniform attack of pure Mg discussed earlier.

The time dependence of the corrosion rate of a bulk RS Mg-Al-Zn-Nd alloy obtained from Allied Corp. was also examined. The electrochemical impedance spectrum of a sample was measured periodically for two weeks while it was immersed in unbuffered 3% NaCl. The goal of these experiments was to use R_{ct} to determine a corrosion rate for comparison with that reported for this alloy by Das and Chang from weight-loss measurements (13). One of these impedance spectra is presented in the Nyquist format in Figure 10 with the approximate charge-transfer and polarization resistances labelled. This diagram shows inductive behavior at low frequency, and is similar to the spectrum observed by Epelboin et al. for iron dissolving in sulfuric acid (15). They observed two inductances, which they attributed to the potential dependence of the surface coverage of hydrogen at lower frequencies and of the anodic intermediate species (FeOH) at higher frequencies. Their weight-loss measurements correlated well with R_{ct}. The corrosion rate of the Mg-Al-Zn-Nd alloy determined after several days from R_{ct} compared well with the weight loss value reported by Das and Chang of about 11 mpy. Like the other alloys, this material was attacked uniformly, and R_{ct} changes indicated a decrease in the corrosion rate with time. The corrosion rate measured on the first day was about 20 mpy. This decrease was probably due to an increase in pH at the electrode surface toward a value where thermodynamics predicts that a stable oxide or hydroxide film forms on Mg.

Corrosion Rates of Binary RS Alloys - Figure 11 summarizes the corrosion rates of the binary RS alloys (Table II), measured in pH 9.2 sodium borate using EIS. The value for pure magnesium represents both the as-cast and rapidly solidified conditions; electrochemical techniques revealed no difference in corrosion rate. Post-exposure examination of RS pure Mg, however, showed uniform attack without evidence of undermining. Reproducibility, as measured by standard deviation, varied widely. Standard deviations ranged from about 3% for Mg-15Al to about 40% for Mg-10Zn. Aluminum is the only element which improved the corrosion resistance, causing the rate to decrease as Al content increased. Surface analyses were conducted at the Lockheed Palo Alto Research Laboratory as part of this investigation. Depth profiling (5 keV Ar sputtering) using Auger electron spectroscopy (AES) and x-ray photoelectron spectroscopy (XPS) showed the air-formed oxide on the Mg-Al alloys was a layered structure (5-15 nm thick) composed of MgO/Mg-Al-oxide/substrate, with the oxide (Mg-rich) thinner with increasing Al content. It is likely that this benefit of aluminum is related to the nature of this oxide, the strong tendency for Al to form a stable passive film in this electrolyte, and the lack of galvanic action between Mg and Al in these alloys. These results also show that small additions of lithium do not seriously degrade the corrosion

resistance of pure magnesium. Lithium was examined mainly because it has a low density and can form a new BCC phase. Small amounts of Li added to magnesium caused only a slight increase in the corrosion rate compared to Zn, Ca, and Si, suggesting that lithium additions of about 2 wt.% are tolerable.

Zinc had a somewhat anomalous effect on the corrosion behavior of Mg, as evidenced by the peak seen in Figure 11 at the 18.6 wt.% level. This intermediate addition caused a drastic increase in the corrosion rate, while additions of 4.8% and 27.5% had corrosion rates only slightly higher than that measured for pure Mg. AES sputter profiling of Mg-Zn alloys indicated the presence of oxide films whose thicknesses, in the range 6-18 nm, decreased with increasing Zn content. These air-formed films were magnesium-rich and contained little or no zinc. Exposure to sodium borate (20 or 60 minutes) produced a zinc-rich surface layer (100-400 nm) above an oxide layer (300-1100 nm) containing little or no zinc. The 27.5% Zn content is lower than that required for glass formation (42-65 wt.% Zn), so the role of zinc at high levels is unclear and warrants further study. For alloys of practical interest to this study, the Zn content must be small due to its high density, and these corrosion data suggest that low zinc levels are not as harmful as similar levels of silicon and calcium.

Calcium appears to have an effect similar to zinc, causing the corrosion rate to increase to a maximum, and then decrease with further additions. This raises the question of whether Mg-Ca alloys with calcium contents higher than the 11 wt.% maximum studied here have corrosion rates lower than pure Mg. While weight considerations make high concentrations undesirable for zinc, calcium has a density of about 1.5 g/cm^3, and may therefore be added liberally without sacrificing low density. Additional studies of these alloys seem necessary to determine the causes of the maxima in the corrosion rate curves for Ca and Zn, and to further investigate the Mg-Si and Mg-Li systems for evidence of this effect. Note, however, that alloys high in calcium and silicon are unsuitable for structural applications due to their poor strength and/or ductility. Magnesium alloys high in lithium may have greater applicability and are the subject of a current study by the Aluminum Company of America (20).

Passivity and Breakdown of Alloy AZ61 - The effect of RSP on alloy AZ61 (Mg-6Al-1Zn) was examined using anodic polarization scans in the presence of chloride. The electrolytes used were 0.05M Na borate (pH 9.2) and 0.025M Na carbonate/0.025M Na bicarbonate (pH 10.0) with 100 ppm, 1000 ppm, or 3.5% NaCl. Scans were reproduced closely in duplicate experiments, particularly in the active region, where curves were virtually identical. Figure 12 presents anodic polarization data for cast and RS AZ61 ribbon in the carbonate buffer with 100 ppm NaCl. The characteristic parameters i_p and E_b are indicated. The passive current density, i_p, is an indication of the protective film's ability to maintain a low corrosion rate in the passive regime. The breakdown potential, E_b, is one measure of the resistance of a metal or alloy to attack by an aggressive species; a higher (more positive) value of E_b indicates better resistance. E_b is a parameter which is dependent on experimental conditions, but is

generally considered the potential at which the current begins to rise above its passive value due to breakdown of the film and subsequent pit propagation. Previous studies revealed that i_p and open-circuit dissolution rate were affected little by RSP (21). However, some interesting improvements are seen in resistance to attack by Cl^-.

Figure 12 shows that the breakdown potential for the RS AZ61 is about 200 mV higher than that for the cast material. This 200 mV improvement was observed in the carbonate buffer at all Cl^- levels. Figure 13 presents the results of similar experiments conducted in the borate buffer with 100 ppm NaCl. The breakdown potentials do not indicate any improvement for the RS material, which was the case for all chloride levels. However, the current increase in the region marked "x" of the curve for the cast material at about -1.5 V (Figure 13) indicates pit initiation. These pits were also observed visually, and hydrogen evolution accompanied their formation. Continued polarization was not accompanied by a large current increase which normally occurs when the breakdown potential is exceeded, probably due to the fact that the current involved in the slow propagation of these pits is not large compared to i_p. The implication is that the borate-formed film more readily nucleates pits and is probably less stable on the cast AZ61. Figure 13 shows that the melt-spun alloy began pitting and the cast alloy developed new pits at about +0.4 V, this value being slightly higher for the cast material. Standard deviations for the two breakdown potentials at -1.5 V and +0.4 V were 10 mV and 45 mV, respectively. The average value for i_p for six scans varied between about 1 and 1.8 mA/cm^2.

The two types of pits formed on cast AZ61 were visible after removal of the corrosion products and are pictured in Figure 14. The hemispherical pits initiated at -1.5 V (right) appeared as defects in the black film which formed in this potential region. While a 1 cm^2 cast sample typically had 50 or more of these pits, an equal area of RS material formed a few at most. The larger attacked area (left), is made up of many irregularly shaped pits, and these were seen on both the cast and RS specimens at +0.4 V. The observed improvements may result from increased microstructural homogeneity or the formation of glassy films, possibly a combination of both. As discussed in the experimental details, the highly refined microstructure of the RS AZ61 bore little resemblance to its parent cast material. Changes in the distribution, density, or identity of secondary phases may be responsible for these differences in localized corrosion behavior. Similar observations were made by Bertocci and Kruger, who used an electrochemical noise technique to examine the passive films on Fe-Cr-Ni alloys (22). They showed that the film on a glassy alloy was more resistant to breakdown/repassivation events than that on its crystalline counterpart, but little change in overall current density was observed. Hagans recently studied $Mg_{70}Zn_{30}$ metallic glass and pure Mg in a pH 9.3 boric/borate buffer with 1000 ppm Cl^- (10). The metallic glass formed a more protective film than the pure metal, as reflected in a 400 mV improvement in the breakdown potential and a lower passive current density.

Summary

Electrochemical impedance data for magnesium in pH 9.2 sodium borate were characteristic of a system controlled by charge transfer. The data showed a single time constant typical of a parallel RC circuit in series with another resistance, a simple circuit model representing a freely corroding surface in series with the electrolyte resistance and commonly called a Randles circuit. Although the impedance spectra of some of the magnesium alloys examined were similar to that of pure magnesium, most displayed additional time constants at low frequency (less than about 10 Hz). The low-frequency behavior was either capacitive, inductive, or characteristic of diffusion effects depending on the alloy composition. Comparison of corrosion rates of bulk magnesium and several alloys calculated from gravimetric, electrochemical impedance, and linear polarization measurements showed that the charge-transfer resistance could be used to accurately calculate a general corrosion rate for these materials. The requirement of uniform attack, at least on a micron scale, is a stringent one. The susceptibility of magnesium to internal galvanic attack can promote the undermining of small particles, as in the case of the "pure" magnesium examined in this work. This can result in a weight loss much greater than that due solely to electrochemical dissolution.

Effects of Al, Ca, Li, Si, and Zn on the corrosion rate of rapidly solidified magnesium in pH 9.2 sodium borate were evaluated using EIS. These measurements showed that the presence of aluminum is beneficial to RS magnesium, while the other elements caused varying increases in corrosion rate. Zinc and lithium were only slightly detrimental at low concentrations. Anodic polarization studies of RS and as-cast commercial alloy AZ61 conducted in sodium borate (pH 9.2) and sodium carbonate/bicarbonate (pH 10.0) with 100 ppm to 3.5 wt.% NaCl indicated that the RS ribbon forms a more protective film* than the cast material in these solutions. The benefit may reflect the homogeneous character of the RS substrate, possibly combined with a tendency toward formation of a less crystalline film (i.e. fewer defects).

*X-ray absorption (EXAFS) studies examining the nature of this film have been carried out by JHU and NIST and will soon be submitted for publication.

Acknowledgements

This work was supported by the Air Force Office of Scientific Research under Contract No. F496620-86-C-0014 and by the Air Force Wright Aeronautical Laboratories under Contract No. F33615-85-C-5032. Thanks are also extended to Anne Joshi and Al Davinroy of the Lockheed Palo Alto Research Laboratory, Patrick Hagans of Dow Chemical U.S.A., C.F. Chang of Allied Corporation, Robert Shull of the National Institute of Standards

and Technology, and Robert Kelly and Deniol Tanaka of The Johns Hopkins University. Sponsorship of the JHU Corrosion and Electrochemistry Research Laboratory by EG&G Princeton Applied Research is gratefully acknowledged.

References

1) H.H. Uhlig and R. Winston Revie, Corrosion and Corrosion Control (New York: John Wiley & Sons, Inc., 1985), Chapter 20.

2) G.R. Hoey and M. Cohen, "Corrosion of Anodically and Cathodically Polarized Magnesium in Aqueous Media," *This Journal*, 105 (5) (1958), 245-250.

3) J.H. James, "Rate of Solution of Magnesium in Acids," *J. Am. Chem. Soc.*, 65 (1) (1943), 39-41.

4) E.J. Casey and R.E. Bergeron, "On the Mechanism of the Dissolution of Magnesium in Acidic Salt Solutions," *Can. J. Chem.*, 31 (9) (1953), 849-867.

5) B. Roald and W. Beck, "The Dissolution of Magnesium in Hydrochloric Acid," *This Journal*, 98 (7) (1951), 277-290.

6) K.G. Cowan and J.A. Harrison, "The Dissolution of Magnesium in Cl^- and F^- Containing Aqueous Solutions," *Electrochim. Acta*, 24 (1979), 301-308.

7) P.L. Hagans, "Electrochemical Study of the Passivation of Mg, Al, and Mg Alloy AZ91B," *Electrochem. Soc. Extended Abstracts*, 83 (1) (1983), 112-113.

8) J.D. Hanawalt, C.E. Nelson, and J.A. Peloubet, "Corrosion Studies of Magnesium and Its Alloys," *Trans. AIME*, 147 (1942), 273-299.

9) K.N. Reicheck, K.J. Clark, and J.E. Hillis, "Controlling the Salt Water Corrosion Performance of Magnesium AZ91 Alloy," International Congress and Exposition, Soc. of Automot. Eng., 1985, Paper No. 850417.

10) P.L. Hagans, "Electrochemical Study of the Passivation and Passive Film Breakdown of $Mg_{70}Zn_{30}$ Metallic Glass," *Mater. Res. Soc. Symp. Proc.*, 80 (1987), 113-120.

11) K. Ogura and K. Sato, "Role of Oxygen-Containing Species in the Passivation of Iron," in Passivity of Metals, R.P. Frankenthal and J. Kruger, eds. (Princeton, NJ: The Electrochemical Society, Inc., 1978),463-478.

12) S.K. Das and C.F. Chang, "High Strength Magnesium Alloys by Rapid Solidification Processing," in Rapidly Solidified Crystalline Alloys, S.K. Das, B.H. Kear, and C.M. Adam, eds. (Warrendale, PA: TMS-AIME, 1985), 137-156.

13) C.F. Chang, S.K. Das, D. Raybould, and A. Brown, "Corrosion Resistant High Strength Magnesium Alloys by RSP," *Met. Powder Rep.*, 41 (4) (1986), 302-308.

14) H. Jones, A. Joshi, R.G. Rowe, and F.H. Froes, "The Current Status of Rapid Solidification of Magnesium-Base and Titanium-Base Alloys," *The Int. J. Powder Met.*, 23 (1) (1987), 13-24.

15) I. Epelboin, C. Gabrielli, M. Keddam, and H. Takenouti, "Alternating-Current Impedance Measurements Applied to Corrosion-Rate Determination," in Electrochemical Corrosion Testing, ASTM 727, F. Mansfeld and U. Bertocci, eds. (Philadelphia, PA: ASTM, 1981), 150-166.

16) G.A. Marsh and E. Schaschl, "The Difference Effect and the Chunk Effect," *This Journal*, 107 (12) (1960), 960-965.

17) M.E. Straumanis and B.K. Bhatia, "Disintegration of Magnesium While Dissolving Anodically in Neutral and Acidic Solutions," *This Journal*, 110 (5) (1963), 357-360.

18) W.J. James, M.E. Straumanis, B.K. Bhatia, and J.W. Johnson, "The Difference Effect on Magnesium Dissolving in Acids," *This Journal*, 110 (11) (1963), 1117-1120.

19) R.L. Petty, W. Davidson, and J. Kleinberg, "The Anodic Oxidation of Magnesium Metal: Evidence for the Existence of Unipositive Magnesium," *J. Am. Chem. Soc.*, 76 (1954), 363-366.

20) R.K. Weiss, "A Study of Mg-Li Alloys with Two Phase (HCP + BCC) structures," Proceedings of the 1988 TMS-AIME symposium entitled Advances in Magnesium Alloys and Composites (Warrendale, PA: TMS-AIME, in press).

21) G.L. Makar, J. Kruger, and A. Joshi, "The Effect of Alloying Elements on the Corrosion Resistance of Rapidly Solidified Magnesium Alloys, Proceedings of the TMS-AIME symposium entitled Advances in Magnesium Alloys and Composites (Warrendale, PA: TMS-AIME, in press).

22) U. Bertocci and J. Kruger, "Studies of Passive Film Breakdown by Detection and Analysis of Electrochemical Noise," *Surf. Sci.*, 101 (1980), 608-618.

Table I. Chemical Analysis of High-Purity Magnesium.

Element	Wt. Percent	Element	Wt. Percent
Al	0.002	Ni	0.0002
Ca	0.001	Pb	0.001
Cd	<0.0001	Si	0.002
Cu	0.0003	Sn	<0.001
Fe	0.001	Zn	0.006
Mn	0.002	Mg	Balance

Table I. Chemical analysis of the high-purity (99.98%) magnesium used in this study. (Provided by the supplier.)

Table II. RS Binary Alloys Examined in This Study.

ALLOYING ELEMENT				
Aluminum	Zinc	Lithium	Calcium	Silicon
Mg-14.4Al	Mg-4.8Zn	Mg-2.0Li	Mg-5.5Ca	Mg-1.7Si
Mg-28.8Al	Mg-18.6Zn	Mg-7.7Li	Mg-11.3Ca	
Mg-42.8Al	Mg-27.5Zn	Mg-14.0Li		

*Compositions are given in weight percent.

Table II. Binary melt-spun alloys examined in this study. Compositions are given in weight percent.

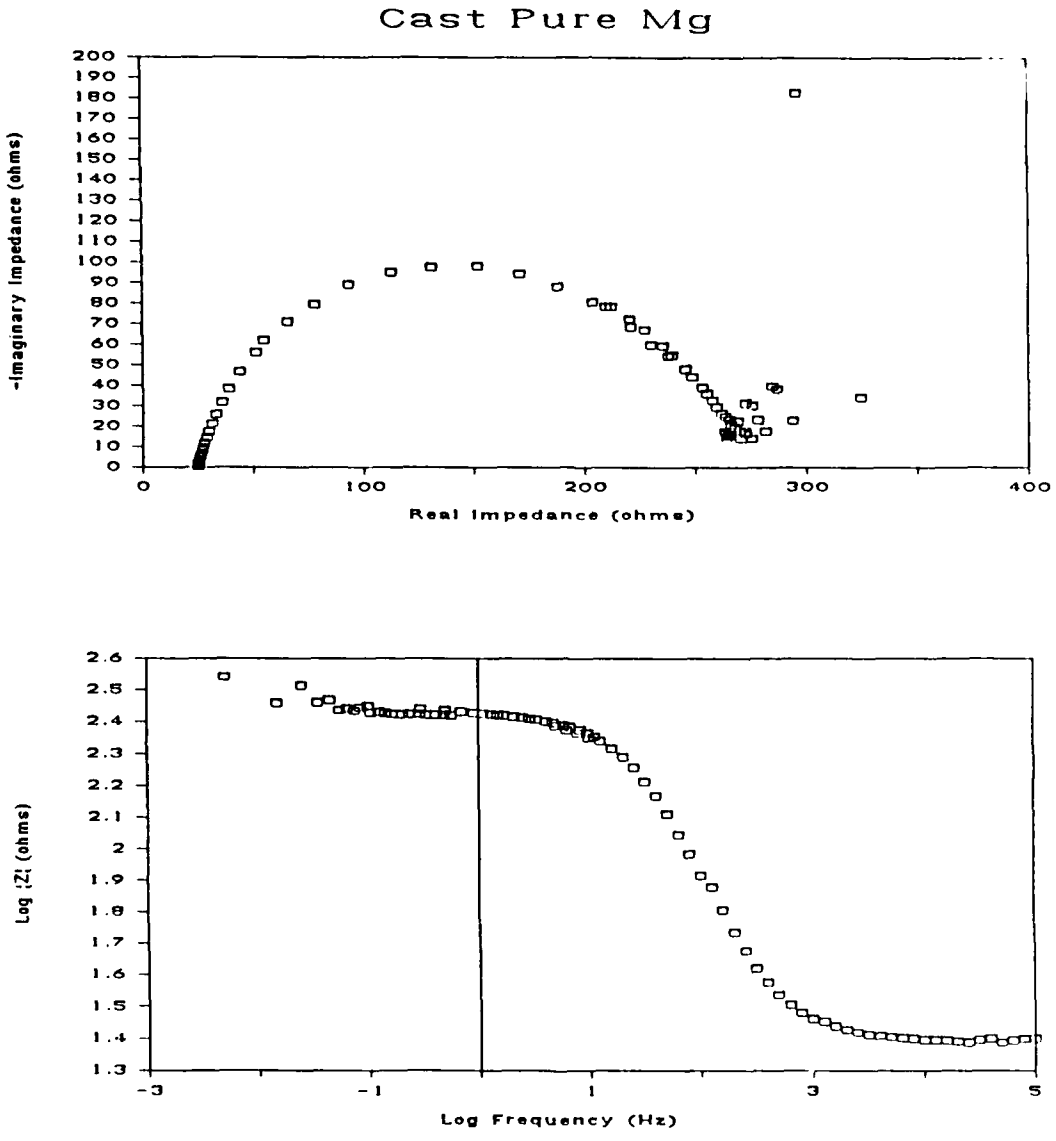

Figure 1 - Electrochemical impedance data for cast pure magnesium in pH 9.2 sodium borate presented in the Nyquist format (top) and Bode magnitude format (bottom).

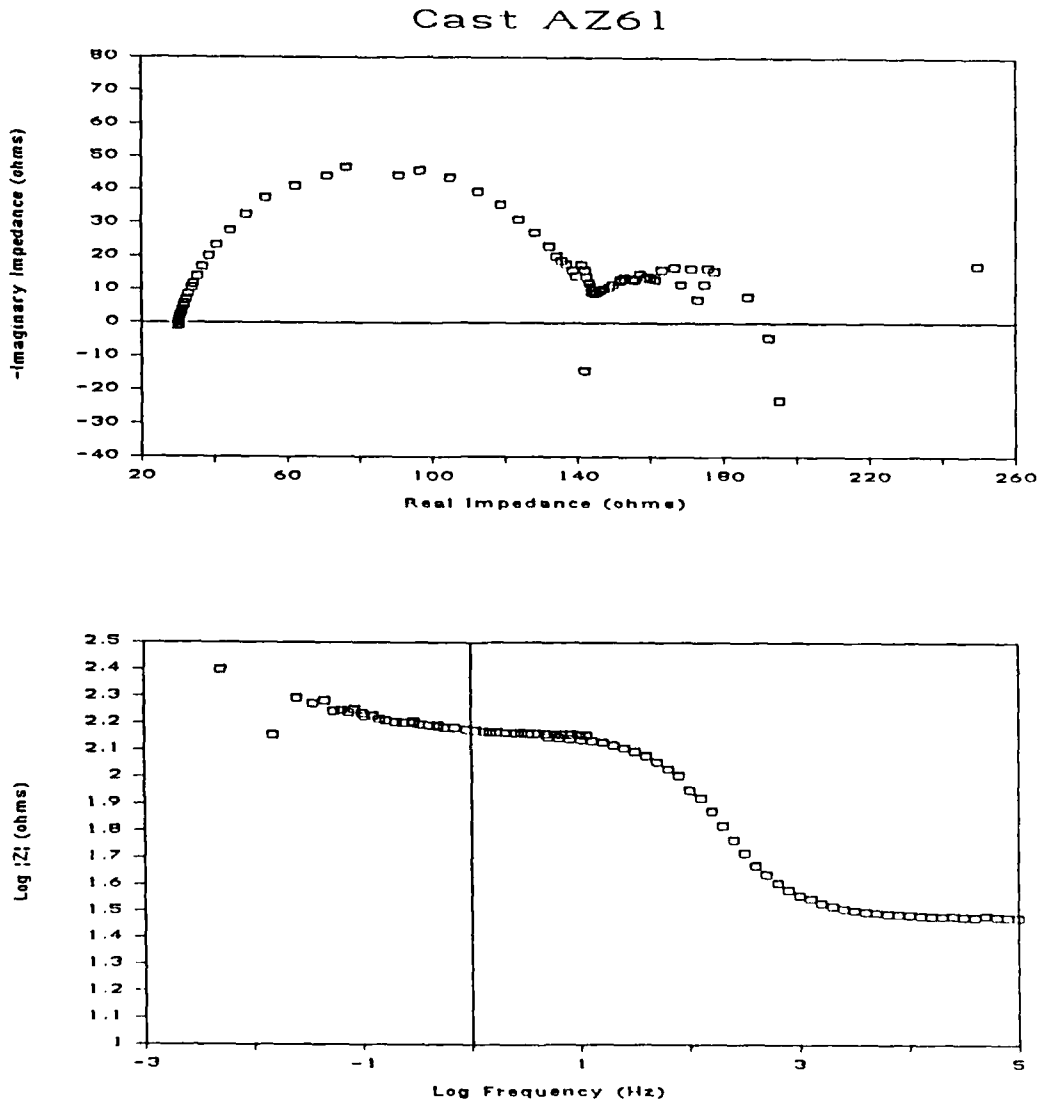

Figure 2 - Electrochemical impedance data for cast alloy AZ61 (Mg-6Al-1Zn) in pH 9.2 sodium borate presented in the Nyquist format (top) and Bode magnitude format (bottom).

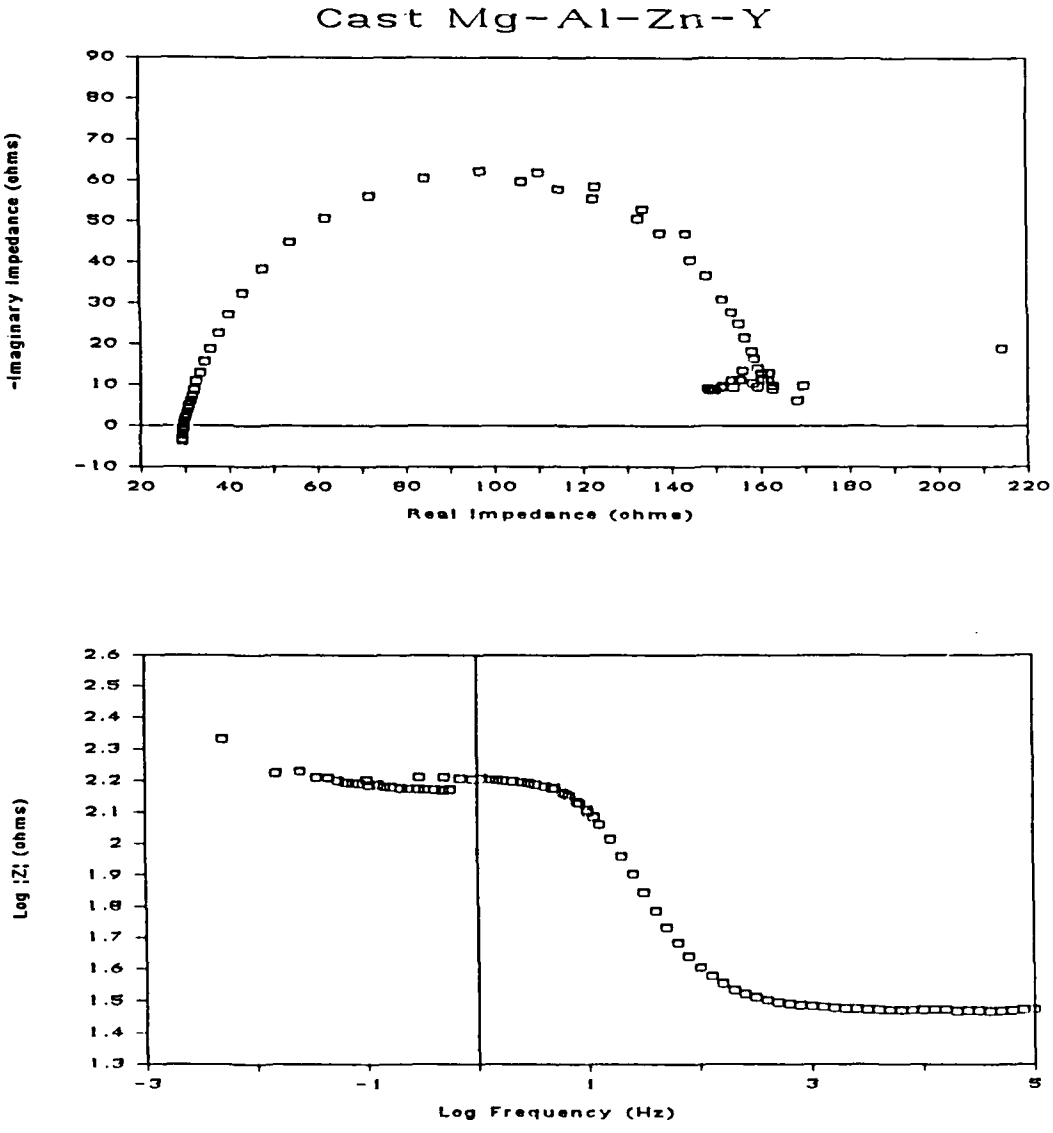

Figure 3 - Electrochemical impedance data for cast Mg-Al-Zn-Y alloy in pH 9.2 sodium borate presented in the Nyquist format (top) and Bode magnitude format (bottom).

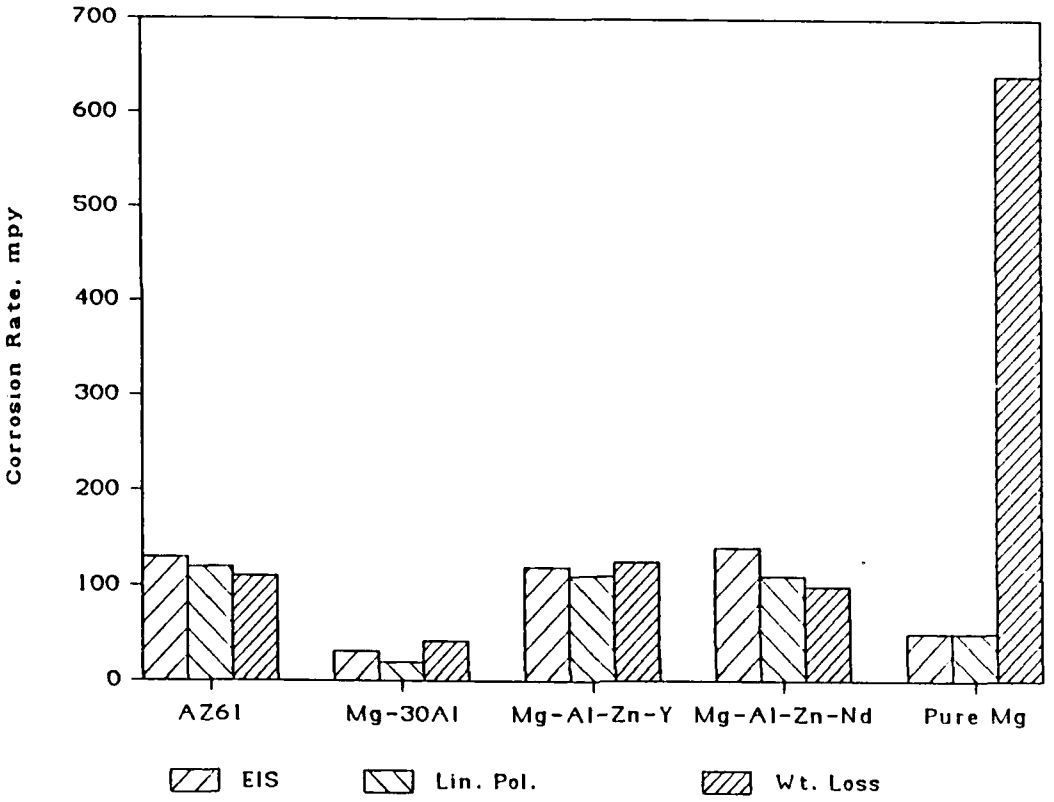

Figure 4 - Comparison of corrosion rates of bulk alloys in pH 9.2 sodium borate determined from electrochemical and gravimetric techniques. The exact compositions of the Mg-Al-Zn-RE alloys are proprietary.

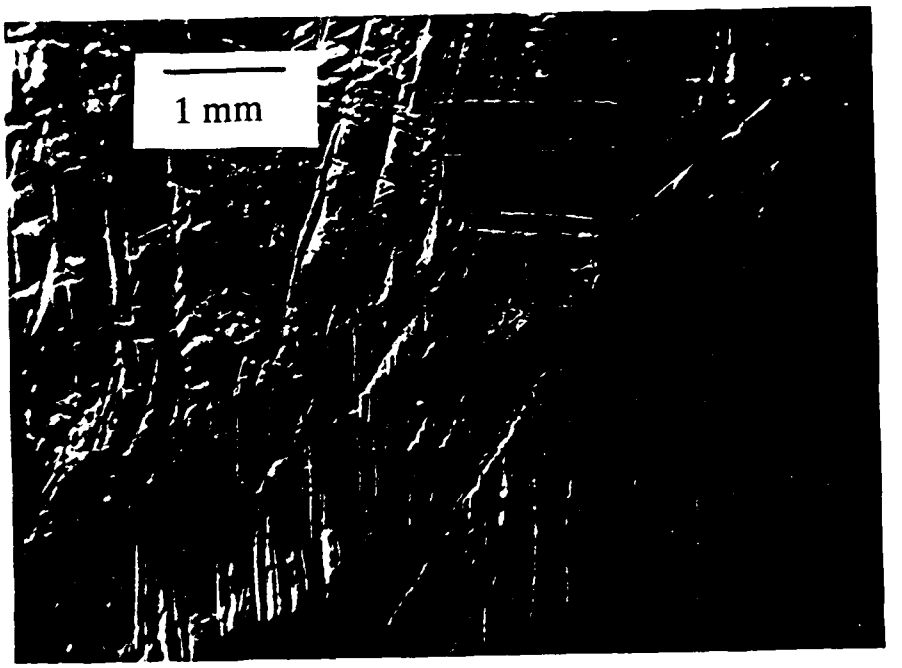

Figure 5 SEM photomicrograph of cast pure magnesium surface after one-week immersion in pH 9.2 sodium borate and subsequent removal of corrosion products.

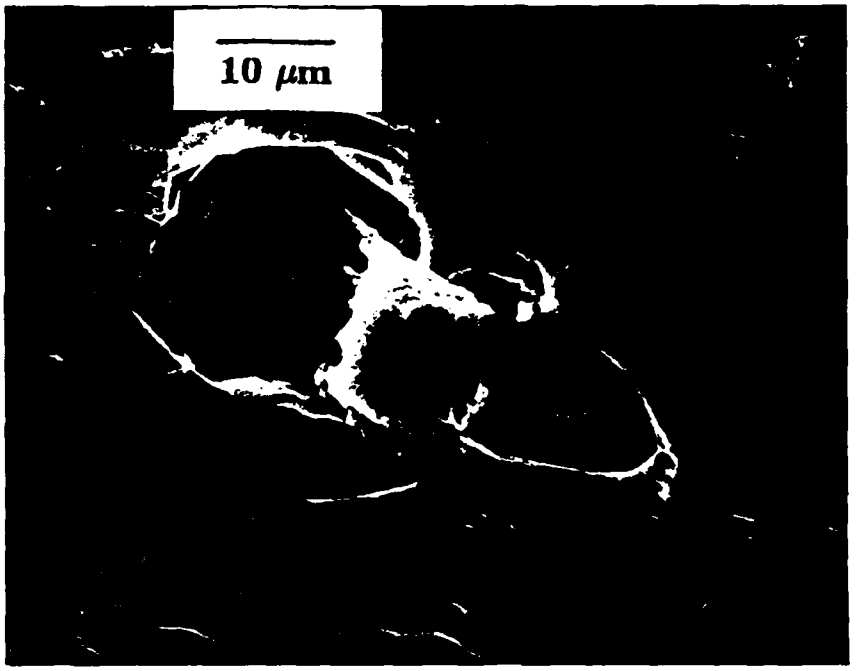

Figure 6 SEM photomicrograph of cast pure magnesium surface after one-week immersion in pH 9.2 sodium borate and subsequent removal of corrosion products. Shown is a particle, roughly 10 μm in diameter, which has been partially undermined by the surrounding matrix.

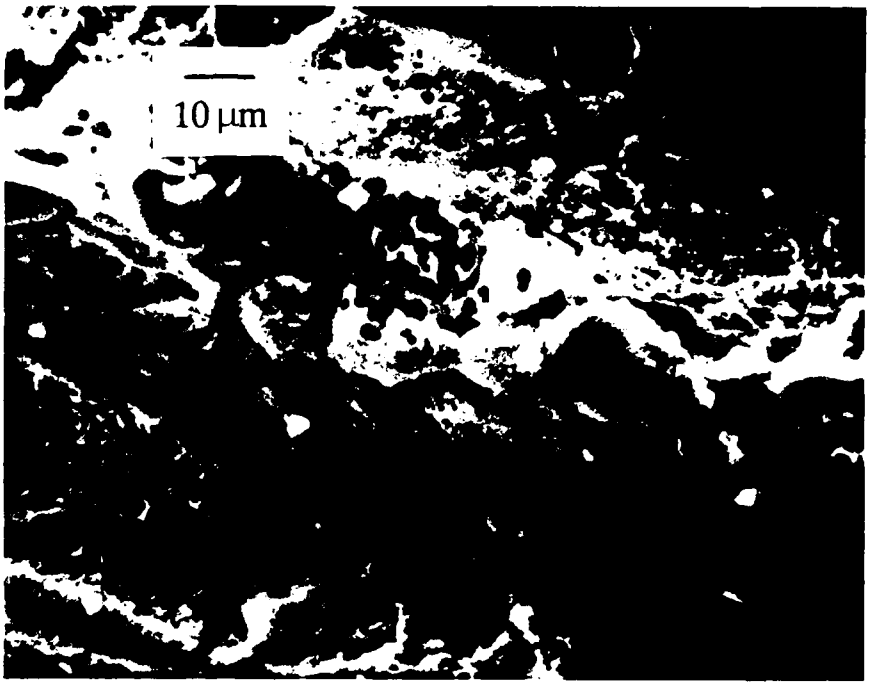

Figure 7 SEM photomicrograph of cast AZ61 surface after one-week immersion in pH 9.2 sodium borate and subsequent removal of corrosion products.

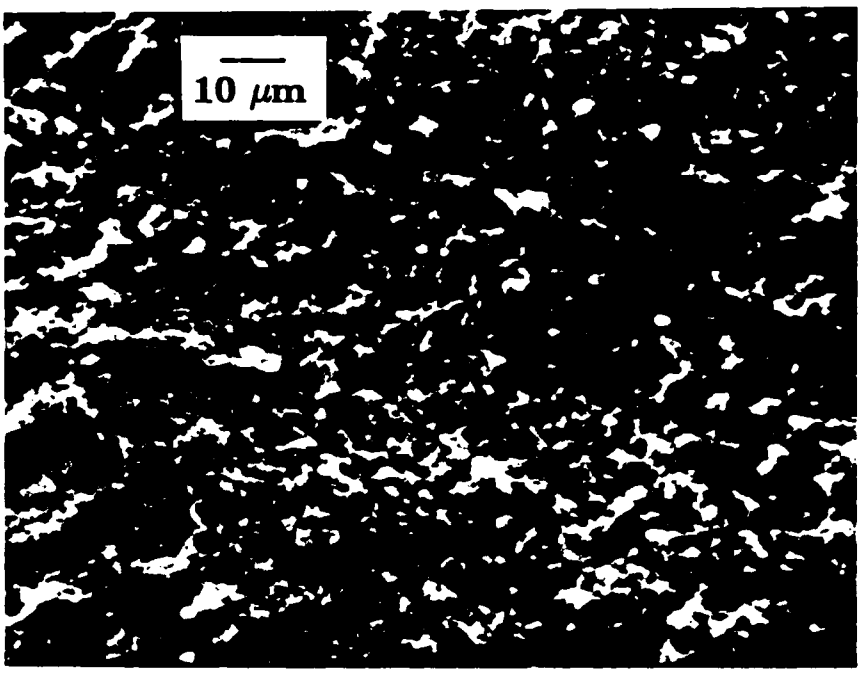

Figure 8 SEM photomicrograph of cast Mg-Al-Zn-Y surface after one-week immersion in pH 9.2 sodium borate and subsequent removal of corrosion products.

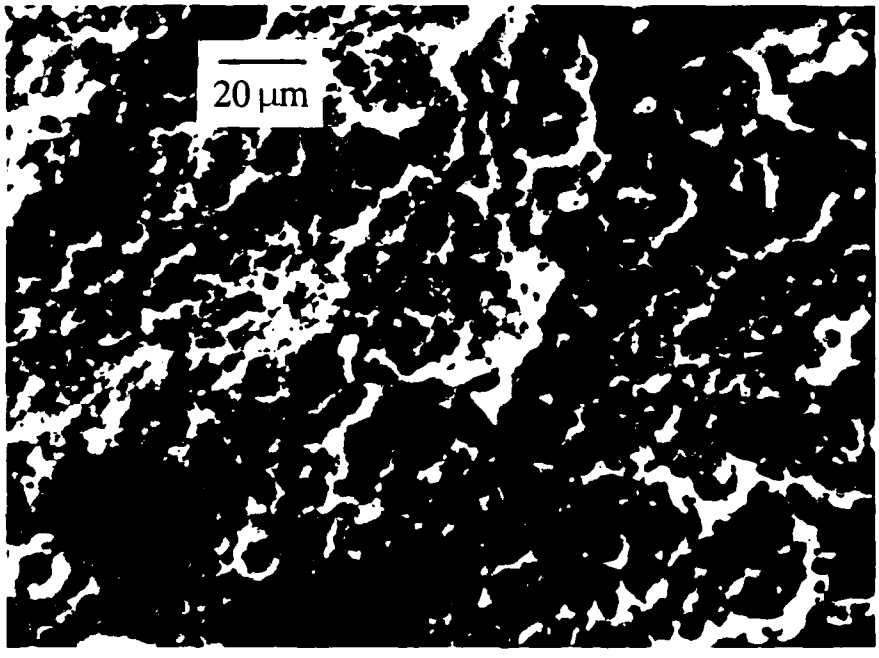

Figure 9 SEM photomicrograph of RS Mg-14.4Al surface after several hours in pH 9.2 sodium borate and subsequent removal of corrosion products.

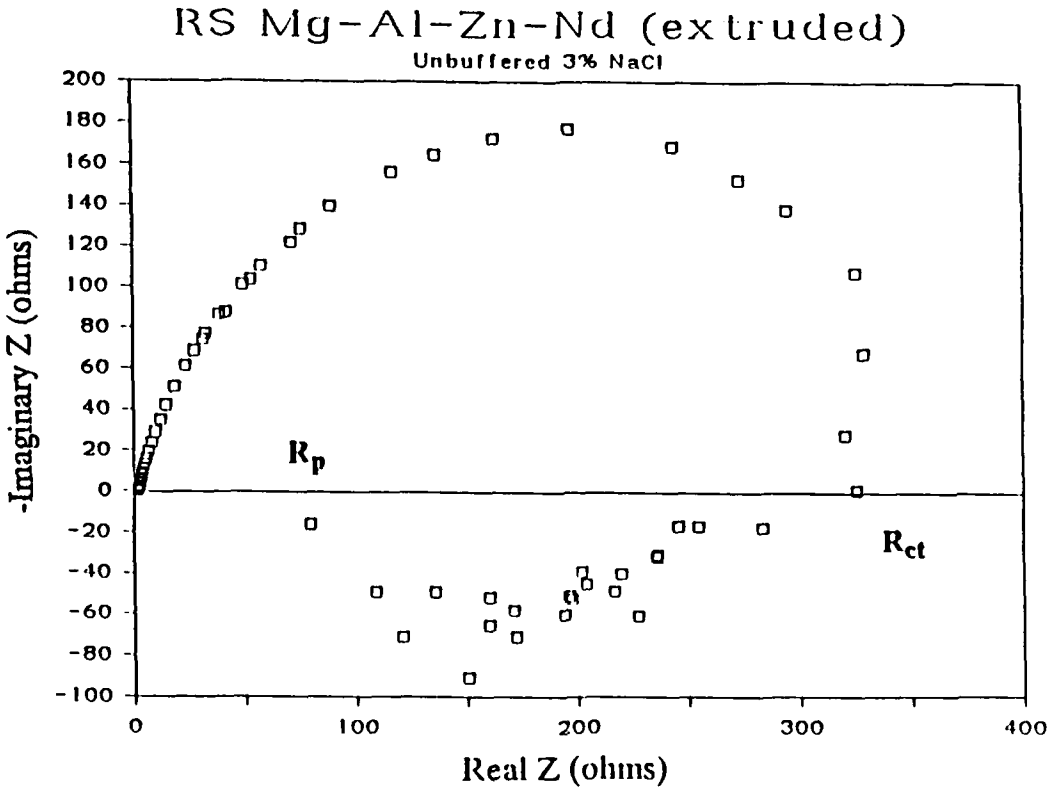

Figure 10 - Nyquist plot of electrochemical impedance data for RS Mg-Al-Zn-Nd (extruded) after 14 days in unbuffered 3% sodium chloride showing inductive behavior at low frequency.

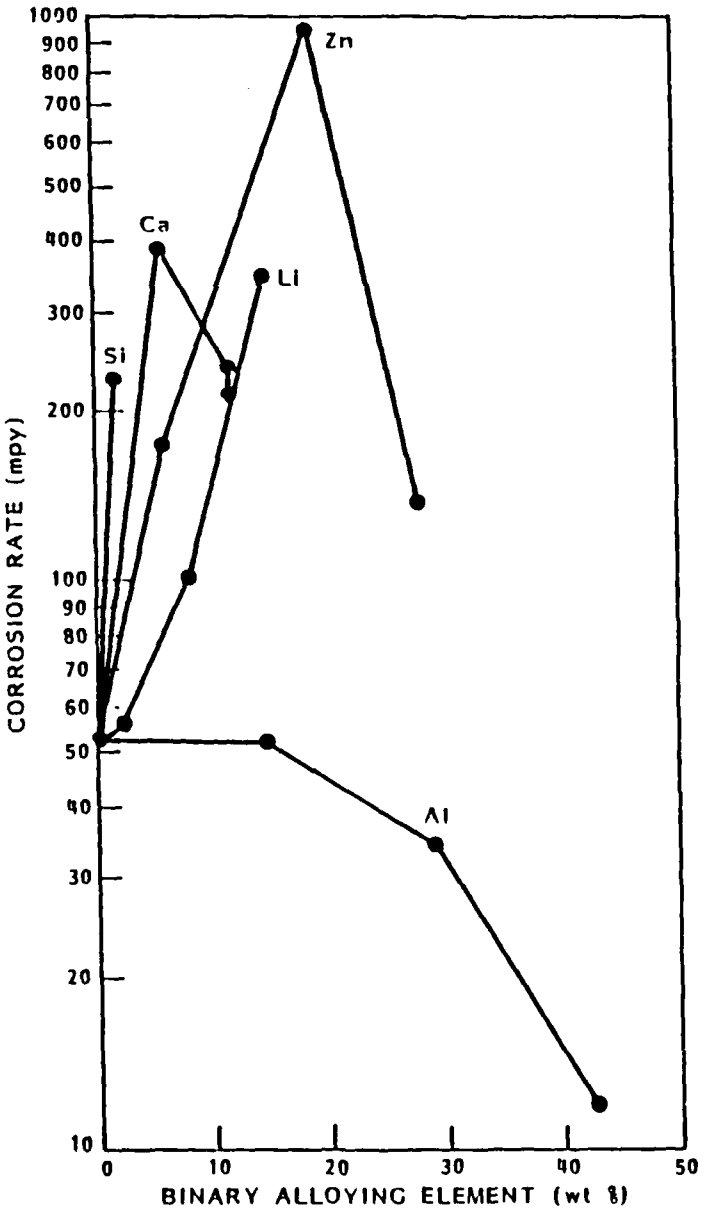

Figure 11 Corrosion rates of binary RS magnesium alloys determined using EIS.

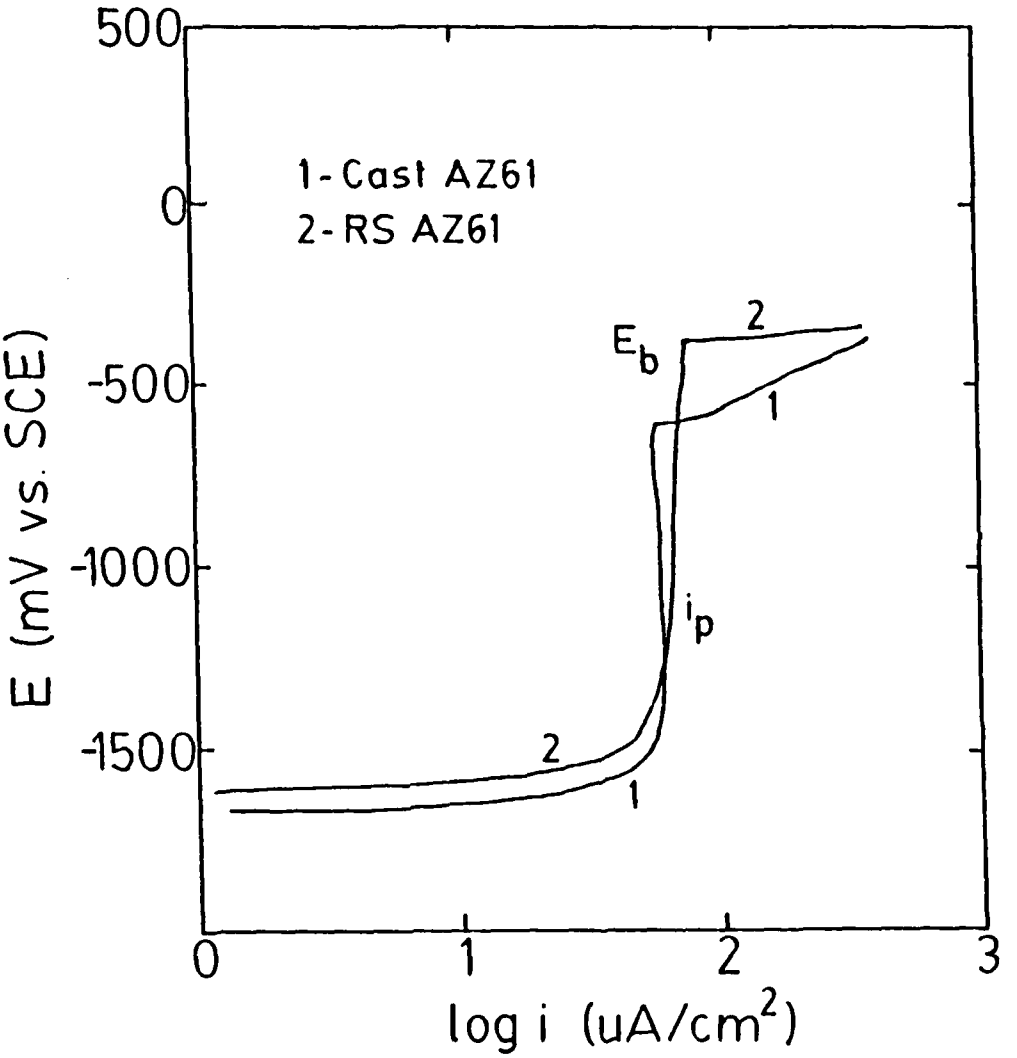

Figure 12 Anodic polarization scans for cast and RS AZ61 in pH 10.0 sodium carbonate/sodium bicarbonate with 100 ppm NaCl.

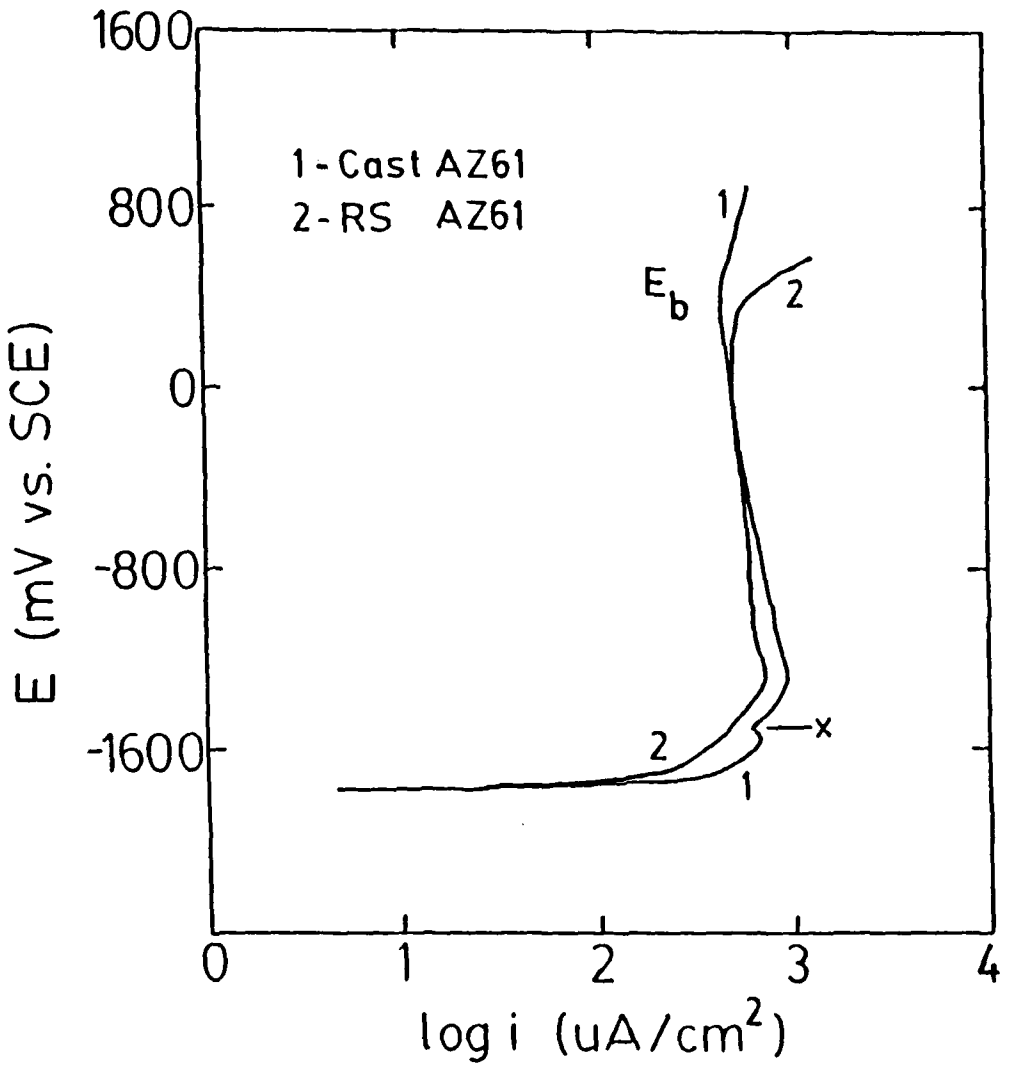

Figure 13 Anodic polarization scans for cast and RS AZ61 in pH 9.2 sodium borate with 100 ppm NaCl.

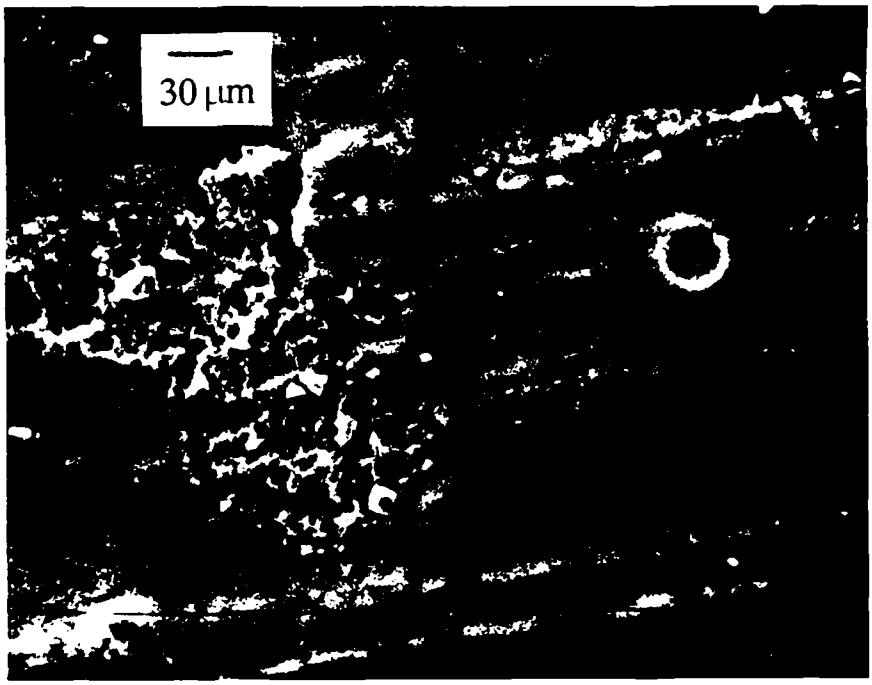

Figure 14 - SEM photomicrograph showing pitted areas on cast AZ61 after anodic polarization scan in pH 9.2 sodium borate containing 100 ppm NaCl. Removal of corrosion product reveals pits formed at -1.5V SCE (right) and at +0.4V SCE (left).